ADVANCED POLARIMETRIC CONCEPTS – PART 1
(*Polarimetric Target Description, Speckle filtering and Decomposition Theorems*)

Eric POTTIER[(1)], Jong-Sen LEE[(2)], Laurent FERRO-FAMIL[(1)]

(1) **I.E.T.R – UMR CNRS 6164 – University of Rennes1**
Image and Remote Sensing Department, SAPHIR Team
Campus de Beaulieu, Bat 11D, 263 Av Gal Leclerc
F-35042 Rennes cedex, France
e-mail : eric.pottier@univ-rennes1.fr,
laurent.ferro-famil@univ-rennes1.fr

(2) **Naval Research Laboratory**
Remote Sensing Division
Washington, DC 20375-5351 USA
e-mail : lee@ccf.nrl.navy.mil

1 INTRODUCTION

There is currently a great deal of interest in the use of polarimetry for radar remote sensing. In this context, different and important objectives are to classify Earth terrain components within a fully polarimetric SAR image and then extract physical information from the observed scattering of microwaves by surface and volume structures. The most important observable measured by such radar systems is the 3x3-coherency matrix [*T*]. This matrix accounts for local variations in the scattering matrix and is the lowest order operator suitable to extract polarimetric parameters for distributed scatterers in the presence of additive (system) and/or multiplicative (speckle) noise. In the first part of this paper, the most important Target Polarimetry descriptors: Sinclair Matrix, target vectors, coherency matrix and the covariance matrix as well are presented, their interconnections and equivalences will be shown together with the respective transformations.

Speckle appearing in synthetic aperture radar (SAR) images is due to the coherent interference of waves reflected from many elementary scatterers and causes degradation and makes automatic image segmentation and scene description difficult. The speckle reduction problem is more complicated for polarimetric SAR than a single polarization SAR, because of the difficulties of preserving polarimetric properties and of dealing with the cross-product terms. The first part of this paper is ended by a presentation and a description of polarimetric speckle filters preserving polarimetric properties and statistical correlation between channels, not introducing crosstalk, and not degrading the image quality. The impact of using this polarimetric speckle filtering on terrain classification is quite dramatic in boosting classification performance.

Many targets of interest in radar remote sensing require a multivariate statistical description due to the combination of coherent speckle noise and random vector scattering effects from surface and volume. For such targets, it is of interest to generate the concept of an average or dominant scattering mechanism for the purposes of classification or inversion of scattering data. Target Decomposition theorems are aimed at providing such an interpretation based on sensible physical constraints such as the average target being invariant to changes in wave polarization basis. Among the existing Polarimetric Target Decomposition theorems - coherent (Krogager, Cameron ...), non-coherent (Huynen, Barnes ...) model-based decomposition (Freeman) or eigenvector-based decomposition (Cloude, Van Zyl) - the H/A/$\underline{\alpha}$ Decomposition Theorem, proposed by *S.R. Cloude* and *E. Pottier in 1997* for extracting average parameters from experimental data is presented and discussed. Based on an eigenvalues analysis of the coherency matrix, this decomposition theorem employs a 3-level Bernoulli statistical model to generate estimates of the average target scattering matrix parameters.

2 POLARIMETRIC TARGET DESCRIPTORS

2.1 TARGET VECTOR FOR BACKSCATTER PROBLEMS

Radar Polarimetry (Polar: polarization Metry: measure) is the science of acquiring, processing and analysing the polarization state of an electromagnetic field. The polarization information contained in the waves

Pottier, E.; Lee, J.-S.; Ferro-Famil, L. (2007) Advanced Polarimetric Concepts – Part 1 (Polarimetric Target Description, Speckle filtering and Decomposition Theorems). In *Radar Polarimetry and Interferometry* (pp. 6-1 – 6-30). Educational Notes RTO-EN-SET-081bis, Paper 6. Neuilly-sur-Seine, France: RTO. Available from: http://www.rto.nato.int/abstracts.asp.

backscattered from a given medium is highly related to its geometrical structure and orientation as well as to its geophysical properties such as humidity, roughness and conductivity of soils, ...

Radar Polarimetry deals with the full vector nature of polarized electromagnetic waves, and when the wave passes through a medium of changing index of refraction, or when it strikes an object or a scattering surface and it is reflected; then, characteristic information about the reflectivity, shape and orientation of the reflecting body can be obtained from the 2x2 coherent backscattering matrix or Sinclair matrix [Boerner 1998].

An important development in our understanding of how to best extract physical information from the classical 2x2 coherent backscattering matrix [*S*] has been achieved through the construction of system vectors [Cloude 1996][Cloude 1997]. We represent this vectorization of a matrix by the vector *V*(.) built as follows :

$$[S] = \begin{bmatrix} S_{XX} & S_{XY} \\ S_{XY} & S_{YY} \end{bmatrix} \quad \Rightarrow \quad \underline{k} = V([S]) = \frac{1}{2} Trace\left([S][\psi]\right) \tag{1}$$

where *Trace*([*A*]) is the sum of the diagonal elements of matrix [*A*] and [ψ] is a set of 2x2 complex basis matrices which are constructed as an orthonormal set under an hermitian inner product [Cloude 1986][Cloude 1996]. There exist in the literature different basis sets, but the special set used to generate 3x3 coherency matrix [*T*] is based on linear combinations arising from the Pauli matrices, and is given by:

$$[\psi] = \left\{ \sqrt{2}\begin{bmatrix} 1 & 0 \\ 0 & 1 \end{bmatrix}, \sqrt{2}\begin{bmatrix} 1 & 0 \\ 0 & -1 \end{bmatrix}, \sqrt{2}\begin{bmatrix} 0 & 1 \\ 1 & 0 \end{bmatrix} \right\} \tag{2}$$

where the factor $\sqrt{2}$ arises from the requirement to keep the norm of the target vector $\underline{k}$ invariant, equal to the Frobenius norm (Span) of the backscattering matrix [*S*], namely the total power scattered by the target. The target vector $\underline{k}$ has the explicit form shown in (3).

$$\underline{k} = \frac{1}{\sqrt{2}} \left[S_{XX} + S_{YY} \quad S_{XX} - S_{YY} \quad 2S_{XY} \right]^T \tag{3}$$

With such a vectorization we can then generate a coherency matrix from the outer product of the target vector $\underline{k}$ with its conjugate transpose. For the monostatic case, the 3x3 hermitian coherency matrix [*T*] has the following parameterisation [Cloude 1996]:

$$[T] = \underline{k} \cdot \underline{k}^{*T} = \begin{bmatrix} 2A_0 & C - jD & H + jG \\ C + jD & B_0 + B & E + jF \\ H - jG & E - jF & B_0 - B \end{bmatrix} \tag{4}$$

where A_0, B_0, B, C, D, E, F, G and H are the « Huynen parameters » identified as phenomenological target parameters interrelated in such a way as to reflect directly the physical source of correlation effects in the target. These nine parameters are useful for general target analysis without reference to any model, and each of them contains real physical target information [Huynen 1970][Pottier 1992].

The parameters A_0, B_0+B and $B_0 - B$, called the « target generators », are connected respectively with the symmetry, irregularity / double bounce and non-symmetry physical properties in the case of a pure target (strong scatterer) [Huynen 1970][Pottier 1992], or related to surface scattering, double-bounce scattering and volume scattering in the case of a distributed target (natural media).

It is thus possible to use these « target generators » to create a color coding for PolSAR images, by assigning respectively the color red for $B_0 + B = |S_{HH} - S_{VV}|$, green for $B_0 - B = |S_{HV}|$, and blue for $2A_0 = |S_{HH} + S_{VV}|$.

For illustration, the well known NASA/JPL AIRSAR L-Band full polarimetric SAR image of San Francisco Bay (1988) and the DLR E-SAR L-Band full polarimetric SAR image of Oberpfaffenhofen (Germany) are shown respectively on Figs. 1 and 2.

Fig. 1 : Pauli color coded image of the San Francisco Bay.

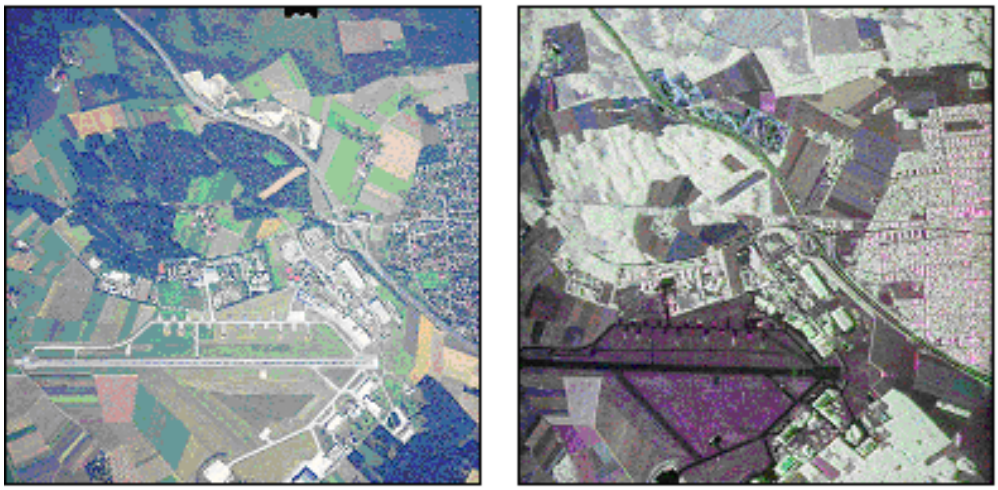

Fig. 2: Optical image and Pauli color coded image over Oberpfaffenhofen (Germany)

In these two displays, the polarimetric channel combinations play an important role in separating ocean surface or agricultural areas (surface scattering), forests, vegetation and trees (volume scattering), and urban areas (double bounce scattering) which composed the different scenes. Called the "Pauli coding representation", this adopted color coding has become today the standard for PolSAR image display.

There exists in the literature a second basis sets, used to generate the 3x3 covariance matrix [C] and is based on a lexicographic combinations of the elements of the Sinclair matrix and is given by [Cloude 1996][Cloude 1997]:

$$\Psi_C = \left\{ 2\begin{bmatrix} 1 & 0 \\ 0 & 0 \end{bmatrix}, 2\sqrt{2}\begin{bmatrix} 0 & 1 \\ 0 & 0 \end{bmatrix}, 2\begin{bmatrix} 0 & 0 \\ 0 & 1 \end{bmatrix} \right\} \tag{7}$$

where the factor $\sqrt{2}$ arises from the requirement to keep the norm of the target vector $\underline{\Omega}$ invariant, equal to the Frobenius norm (Span) of the backscattering matrix [S], namely the total power scattered by the target. The target vector $\underline{\Omega}$ has the explicit form:

$$\underline{\Omega} = \begin{bmatrix} S_{HH} & \sqrt{2}\, S_{HV} & S_{VV} \end{bmatrix}^T \tag{8}$$

With such a vectorization we can then generate a covariance matrix from the outer product of the target vector $\underline{\Omega}$ with its conjugate transpose. For the monostatic case, the 3x3 hermitian covariance matrix [C] has the following parameterisation [Cloude 1996][Cloude 1997]:

$$[C] = \underline{\Omega} \cdot \underline{\Omega}^{*T} = \begin{bmatrix} |S_{HH}|^2 & \sqrt{2}\, S_{HH} S_{HV}^* & S_{HH} S_{VV}^* \\ \sqrt{2}\, S_{HV} S_{HH}^* & 2|S_{HV}|^2 & \sqrt{2}\, S_{HV} S_{VV}^* \\ S_{VV} S_{HH}^* & \sqrt{2}\, S_{VV} S_{HV}^* & |S_{VV}|^2 \end{bmatrix} \tag{9}$$

which can be also expressed in a well-known form given by :

$$[C] = \sigma \begin{bmatrix} 1 & \beta\sqrt{\delta} & \rho\sqrt{\gamma} \\ \beta^*\sqrt{\delta} & \delta & \varepsilon\sqrt{\gamma\delta} \\ \rho^*\sqrt{\gamma} & \varepsilon^*\sqrt{\gamma\delta} & \gamma \end{bmatrix} \tag{10}$$

with :

$$\begin{gathered} \sigma = \left\langle |S_{HH}|^2 \right\rangle \qquad \delta = 2\frac{\left\langle |S_{HV}|^2 \right\rangle}{\left\langle |S_{HH}|^2 \right\rangle} \qquad \gamma = \frac{\left\langle |S_{VV}|^2 \right\rangle}{\left\langle |S_{HH}|^2 \right\rangle} \\ \rho = \frac{\left\langle S_{HH} S_{VV}^* \right\rangle}{\sqrt{\left\langle |S_{HH}|^2 \right\rangle \left\langle |S_{VV}|^2 \right\rangle}} \quad \beta = \frac{\left\langle S_{HH} S_{HV}^* \right\rangle}{\sqrt{\left\langle |S_{HH}|^2 \right\rangle \left\langle |S_{HV}|^2 \right\rangle}} \quad \varepsilon = \frac{\left\langle S_{HV} S_{VV}^* \right\rangle}{\sqrt{\left\langle |S_{HV}|^2 \right\rangle \left\langle |S_{VV}|^2 \right\rangle}} \end{gathered} \tag{11}$$

The two target vectors $\underline{k}$ and $\underline{\Omega}$ are linked together with a unitary transformation which is given by :

$$\underline{k} = \frac{1}{\sqrt{2}} \begin{bmatrix} +1 & 0 & +1 \\ +1 & 0 & -1 \\ 0 & \sqrt{2} & 0 \end{bmatrix} \underline{\Omega} \quad \Leftrightarrow \quad \underline{k} = [U_3]\underline{\Omega} \tag{12}$$

where [U_3] is a special unitary SU(3) matrix. It follows the relation between the coherency matrix [T] and the covariance matrix [C]:

$$[T] = [U_3][C][U_3]^{-1} \tag{13}$$

2.2 ELLIPTICAL POLARISATION BASIS CHANGEMENT OPERATION

In the case of the Sinclair matrix or back-scattering matrix, the elliptical polarisation basis changement operator is given by the following unitary congruence (unitary con-similarity) transformation [Boerner 1998]:

$$[S'] = [U_2(\phi, \tau, \nu)]^T [S][U_2(\phi, \tau, \nu)] \tag{14}$$

where the matrix [U_2] is given by :

$$\begin{aligned} [U(\phi, \tau, \nu)] &= [U(\phi)][U(\tau)][U(\nu)] \\ &= \begin{bmatrix} \cos(\phi) & -\sin(\phi) \\ \sin(\phi) & \cos(\phi) \end{bmatrix} \begin{bmatrix} \cos(\tau) & j\sin(\tau) \\ j\sin(\tau) & \cos(\tau) \end{bmatrix} \begin{bmatrix} e^{-j\nu} & 0 \\ 0 & e^{+j\nu} \end{bmatrix} \end{aligned} \tag{15}$$

where the ν, ϕ, τ parameters correspond to the three geometric parameters of the polarisation ellipse described by the ***first*** or ***principal*** Jones vector of the new basis.

The matrix $[U_2]$ belongs to the SU(2) – Special Unitary 2x2 matrix group constructed from the classical unitary matrices Pauli group given by :

$$\sigma_0 = \begin{bmatrix} 1 & 0 \\ 0 & 1 \end{bmatrix} \quad \sigma_1 = \begin{bmatrix} 1 & 0 \\ 0 & -1 \end{bmatrix} \quad \sigma_2 = \begin{bmatrix} 0 & 1 \\ 1 & 0 \end{bmatrix} \quad \sigma_3 = \begin{bmatrix} 0 & -j \\ j & 0 \end{bmatrix} \tag{16}$$

where the matrices verify $\sigma_i^{-1} = \sigma_i^{T*}$ and $\left|\det(\sigma_i)\right| = 1$.

The group of the special unitary matrices (SU(2)) is defined by [Huynen 1970]:

$$[A] = e^{j\alpha\sigma_p} = \cos(\alpha)\sigma_0 + j\sin(\alpha)\sigma_p \tag{17}$$

It follows :

$$\begin{bmatrix} \cos(\phi) & -\sin(\phi) \\ \sin(\phi) & \cos(\phi) \end{bmatrix} = \cos(\phi)\sigma_0 - j\sin(\phi)\sigma_3 = e^{-j\phi\sigma_3} \tag{18}$$

$$\begin{bmatrix} \cos(\tau) & j\sin(\tau) \\ j\sin(\tau) & \cos(\tau) \end{bmatrix} = \cos(\tau)\sigma_0 + j\sin(\tau)\sigma_2 = e^{+j\tau\sigma_2} \tag{19}$$

$$\begin{bmatrix} e^{+j\nu} & 0 \\ 0 & e^{-j\nu} \end{bmatrix} = cos(\nu)\sigma_0 + jsin(\nu)\sigma_1 = e^{+j\nu\sigma_1} \tag{20}$$

These matrices verify the following properties:

$$[A]^{-1} = [A]^{T*} \quad \text{and} \quad \det[A] = +1 \tag{21}$$

$$e^{-j\phi\sigma_3{}^T} = e^{+j\phi\sigma_3} \quad e^{+j\tau\sigma_2{}^T} = e^{+j\tau\sigma_2} \quad e^{+j\nu\sigma_1{}^T} = e^{+j\nu\sigma_1} \tag{22}$$

$$e^{-j\phi\sigma_3{}^*} = e^{-j\phi\sigma_3} \quad e^{+j\tau\sigma_2{}^*} = e^{-j\tau\sigma_2} \quad e^{+j\nu\sigma_1{}^*} = e^{-j\nu\sigma_1} \tag{23}$$

and:

$$\begin{cases} e^{+j(\alpha+\beta)\sigma_p} = e^{+j\alpha\sigma_p} + e^{+j\beta\sigma_p} \\ \sigma_p e^{+j\alpha\sigma_q} = e^{-j\alpha\sigma_q}\sigma_p \end{cases} \quad \text{with:} \quad \begin{matrix} \sigma_p, \sigma_q \in \{\sigma_1, \sigma_2, \sigma_3\} \\ \sigma_p \neq \sigma_q \end{matrix} \tag{24}$$

This special unitary elliptical basis changement matrix can also be described using the parameters ρ and ξ which correspond to the polarisation ratio of this *first* or *principal* Jones vector of the new basis, and are given by :

$$\rho = \frac{tan(\phi) + j\,tan(\tau)}{1 - j\,tan(\phi)tan(\tau)} \qquad \xi = \nu - arctan(tan(\phi)tan(\tau)) \tag{25}$$

The matrix $[U_2]$ is thus given by :

$$[U_2(\phi,\tau,\nu)] = [U_2(\rho,\xi)] = [U_2(\rho)][U_2(\xi)] = \frac{1}{\sqrt{1+|\rho|^2}} \begin{bmatrix} 1 & -\rho^* \\ \rho & 1 \end{bmatrix} \begin{bmatrix} e^{-j\xi} & 0 \\ 0 & e^{+j\xi} \end{bmatrix} \quad (26)$$

In the case of the 3x3 coherency matrix $[T]$, the elliptical polarisation basis changement operator is given by :

$$[T'] = [U_{3T}(\phi,\tau,\nu)][T][U_{3T}(\phi,\tau,\nu)]^{-1} = [U_{3T}(\rho,\xi)][T][U_{3T}(\rho,\xi)]^{-1} \quad (27)$$

where the matrix $[U_{3T}]$ is given by :

$$\begin{aligned}[U_{3T}(2\phi,2\tau,2\nu)] &= [U_{3T}(2\phi)][U_{3T}(2\tau)][U_{3T}(2\nu)] \\ &= \begin{bmatrix} 1 & 0 & 0 \\ 0 & \cos(2\phi) & \sin(2\phi) \\ 0 & -\sin(2\phi) & \cos(2\phi) \end{bmatrix} \begin{bmatrix} \cos(2\tau) & 0 & j\sin(2\tau) \\ 0 & 1 & 0 \\ j\sin(2\tau) & 0 & \cos(2\tau) \end{bmatrix} \begin{bmatrix} \cos(2\nu) & -j\sin(2\nu) & 0 \\ -j\sin(2\nu) & \cos(2\nu) & 0 \\ 0 & 0 & 1 \end{bmatrix}\end{aligned} \quad (28)$$

where the ν, ϕ, τ parameters correspond to the three geometric parameters of the polarisation ellipse described by the ***first*** or ***principal*** Jones vector of the new basis.

The matrix $[U_{3T}]$ belongs to the SU(3) – Special Unitary 3x3 matrix group. Unfortunately it does not exist any direct mathematical link between the SU(2) group matrices and the SU(3) group matrices. To derive the SU(3) group matrices, we have to deal with the elliptical polarisation basis changement operation, and identify for each SU(2) matrix, its equivalent into the SU(3) group. After some derivations, it follows:

$$[U_2(\phi)] = \begin{bmatrix} \cos(\phi) & -\sin(\phi) \\ \sin(\phi) & \cos(\phi) \end{bmatrix} \Rightarrow [U_{3T}(2\phi)] = \begin{bmatrix} 1 & 0 & 0 \\ 0 & \cos(2\phi) & \sin(2\phi) \\ 0 & -\sin(2\phi) & \cos(2\phi) \end{bmatrix} \quad (29)$$

$$[U_2(\tau)] = \begin{bmatrix} \cos(\tau) & j\sin(\tau) \\ j\sin(\tau) & \cos(\tau) \end{bmatrix} \Rightarrow [U_{3T}(2\tau)] = \begin{bmatrix} \cos(2\tau) & 0 & j\sin(2\tau) \\ 0 & 1 & 0 \\ j\sin(2\tau) & 0 & \cos(2\tau) \end{bmatrix} \quad (30)$$

$$[U_2(\nu)] = \begin{bmatrix} e^{-j\nu} & 0 \\ 0 & e^{+j\nu} \end{bmatrix} \Rightarrow [U_{3T}(2\nu)] = \begin{bmatrix} \cos(2\nu) & -j\sin(2\nu) & 0 \\ -j\sin(2\nu) & \cos(2\nu) & 0 \\ 0 & 0 & 1 \end{bmatrix} \quad (31)$$

This special unitary elliptical basis changement matrix can also be described using the parameters ρ and ξ which correspond to the polarisation ratio of this ***first*** or ***principal*** Jones vector of the new basis, and the matrix $[U_{3T}]$ is thus given by :

$$[U_{3T}(\rho,\xi)] = \frac{1}{1+|\rho|^2} \begin{bmatrix} \cos(2\xi) + \Re e\left(\rho^2 e^{-2j\xi}\right) & -j\sin(2\xi) - j\Im m\left(\rho^2 e^{-2j\xi}\right) & 2j\Im m\left(\rho e^{-2j\xi}\right) \\ -j\sin(2\xi) + j\Im m\left(\rho^2 e^{-2j\xi}\right) & \cos(2\xi) - \Re e\left(\rho^2 e^{-2j\xi}\right) & 2\Re e\left(\rho e^{-2j\xi}\right) \\ 2j\Im m(\rho) & -2\Re e(\rho) & 1-|\rho|^2 \end{bmatrix} \quad (32)$$

In the case of the 3x3 covariance matrix [C], the elliptical polarisation basis changement operator is given by :

$$[C'] = [U_{3C}(\phi,\tau,\nu)][C][U_{3C}(\phi,\tau,\nu)]^{-1} = [U_{3C}(\rho,\xi)][C][U_{3C}(\rho,\xi)]^{-1} \tag{33}$$

The SU(3) unitary transformation group for the covariance matrix is obtained from the SU(3) unitary transformation group for the coherency matrix with:

$$[U_{3C}(2\phi,2\tau,2\nu)] = [U_3][U_{3T}(2\phi,2\tau,2\nu)][U_3]^{-1} \tag{34}$$

where :

$$[U_3] = \frac{1}{\sqrt{2}}\begin{bmatrix} +1 & 0 & +1 \\ +1 & 0 & -1 \\ 0 & \sqrt{2} & 0 \end{bmatrix} \tag{35}$$

Expressed in function of the polarisation ratio parameters (ρ and ξ) the special unitary elliptical basis changement matrix [U_{3C}] can also be written following:

$$[U_{3C}(\rho)] = \frac{1}{1+|\rho|^2}\begin{bmatrix} e^{-2j\xi} & \sqrt{2}\,\rho e^{-2j\xi} & \rho^2 e^{-2j\xi} \\ -\sqrt{2}\,\rho^* & 1-|\rho|^2 & \sqrt{2}\,\rho \\ \rho^{*2} e^{+2j\xi} & -\sqrt{2}\,\rho^* e^{+2j\xi} & e^{+2j\xi} \end{bmatrix} \tag{36}$$

2.3 POLARIMETRIC SAR DATA STATISTICS

A polarimetric radar measures the complete scattering matrix [S] of a medium at a given incidence angle and for a given frequency. This scattering matrix with complex elements can be expressed in a vector form, following :

$$\underline{X} = \begin{bmatrix} S_{HH} & \sqrt{2}S_{HV} & S_{VV} \end{bmatrix}^T \tag{37}$$

where the factor $\sqrt{2}$ arises from the requirement to keep the norm of the target vector $\underline{X}$ an invariant, equal to the Frobenius norm (Span) of the backscattering matrix [S], namely the total power scattered by the target. When the radar illuminates an area of a random surface of many elementary scatterers, the one-look scattering vector $\underline{X}$ can be modeled as having a multivariate complex Gaussian probability density function [Lee 1999b], with :

$$P(\underline{X}) = \frac{1}{\pi^3 |[C]|} e^{-\underline{X}^{*T}[C]^{-1}\underline{X}} \tag{38}$$

where $[C]=E(\underline{X}\,\underline{X}^{T*})$is the hermitian covariance matrix of the scattering vector $\underline{X}$.
As the target vector $\underline{k}$ is constructed from a linear combination of the elements of the scattering vector $\underline{X}$, following :

$$\underline{k} = \frac{1}{\sqrt{2}}\begin{bmatrix} S_{HH}+S_{VV} \\ S_{HH}-S_{VV} \\ 2S_{HV} \end{bmatrix} = \frac{1}{\sqrt{2}}\begin{bmatrix} 1 & 0 & 1 \\ 1 & 0 & -1 \\ 0 & 2 & 0 \end{bmatrix}\begin{bmatrix} S_{HH} \\ \sqrt{2}S_{HV} \\ S_{VV} \end{bmatrix} \tag{39}$$

the elements of the target vector $\underline{k}$ are considered as having the same complex Gaussian distribution than the elements of the scattering vector $\underline{X}$.

POLSAR data are frequently multi-look processed for speckle reduction, or data compression. The relative polarimetric information is thus contained in the expected value of the coherency matrix <[*T*] > representing the spatial-averaged distributed target given by :

$$\langle [T] \rangle = \frac{1}{N} \sum_{i=1}^{N} \underline{k}_i \cdot \underline{k}_i^{*T} = \frac{1}{N} \sum_{i=1}^{N} [T_i] \tag{40}$$

where $[T_i]$ is a single-look coherency matrix of the i^{th} pixel.
It has been shown in [Lee 1999b] that the averaged coherency matrix <[*T*]> has a complex Wishart distribution. The probability density function is given by :

$$P\left(\langle [T] \rangle / [T_m]\right) = \frac{L^{Lp} \left|\langle [T] \rangle\right|^{L-p} e^{-L\,Tr\left([T_m]^{-1}\langle [T] \rangle\right)}}{\pi^{\frac{p(p-1)}{2}} \Gamma(L) \ldots \Gamma(L-p+1) \left|[T_m]\right|^{L}} \tag{41}$$

where $[T_m]$ is global coherency matrix with $[T_m] = E(\underline{k}\,\underline{k}^{T*})$, L is the number of look and p the dimension of the target vector $\underline{k}$, with $\boldsymbol{p}=3$ for the reciprocal case ($S_{HV}=S_{VH}$) and $\boldsymbol{p}=4$ for the non-reciprocal case.

The distribution functions for dual polarization (*HH*, *VH*), (*HV*, *VV*) or (*HH*, *VV*) can be derived from this complex Wishart distribution. For example, if only complex *HH* and *VV* are available, $\boldsymbol{p}$=2, and for single polarization, $\boldsymbol{p}$=1, which reduces (9) to the Chi-square distribution with 2*L* degree of freedom.

For the dual polarization case without phase difference information (|*HH*|, |*VV*|), the probability density function has been derived [Lee 1994a]. Letting $R_1 = <\|S_{HH}\|^2>$ and $R_2 = <\|S_{VV}\|^2>$, we have:

$$p(R_1, R_2) = \frac{n^{n+1} (R_1 R_2)^{\frac{(n-1)}{2}} \exp\left[-\frac{n(R_1/C_{11} + R_2/C_{22})}{1-|\rho_c|^2}\right]}{(C_{11}C_{22})^{(n+1)/2} \Gamma(n)(1-|\rho_c|^2)|\rho_c|^{n-1}} I_{n-1}\left(2n\sqrt{\frac{R_1 R_2}{C_{11}C_{22}}}\frac{|\rho_c|}{1-|\rho_c|^2}\right) \tag{42}$$

where $I_n(\,)$ is the modified Bessel function of the *nth* order, $C_{11} = E[R_1]$ and $C_{22} = E[R_2]$.

3 SPECKLE FILTERING

3.1 NEED FOR SPECKLE FILTERING

Unlike optical remote sensing images, characterized by very neat and uniform features, SAR images are affected by speckle [Goze 1993], [Lee 1980], [Lee 1981a], [Lee 1981b], [Lee 1983], [Lee 1986a], [Lee 1986b], [Lee 1994], [Lee 1997], [Lopes 1990], [Lopes 1993], [Touzi 1994]. Speckle confers to SAR images a granular aspect with random spatial variations. Fig. 3 shows an example of single polarization speckled SAR images.

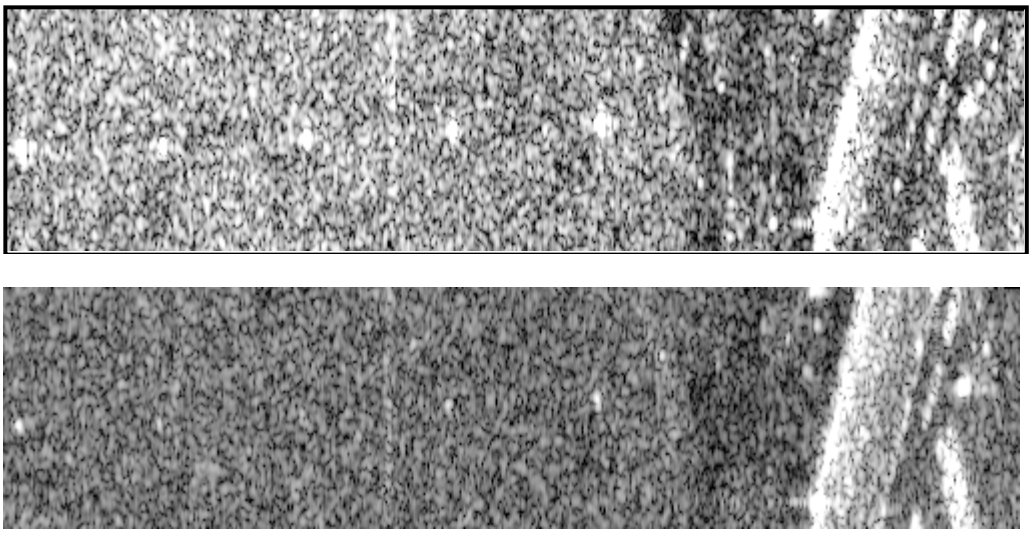

Fig. 3: Single-look $|S_{11}|^2$ (top) and $|S_{12}|^2$ (bottom)images

The intensity images displayed in Fig. 3 show a poor contrast, as well as a random aspect, that reduce the possibilities of visual interpretation and analysis of the scene under consideration.

The discrimination of different natural media by comparing intensity to a fixed threshold leads, in general to numerous errors due to the high variability of SAR speckled response. Speckle phenomenon also affects the phase of scattering coefficients and corrupts polarimetric information.

The image of $Arg(S_{11})$ shown in Fig. 4 indicates that the absolute phase of a scattering coefficient is highly random and does not contain evident information. Speckle does not affect similarly different polarimetric channels, as shown in the between channel relative phase image, $Arg(S_{11}S_{22}^*)$ and in the color coded image, built from the three polarimetric channel intensities, $|S_{11}|^2$, $|S_{12}|^2$ and $R=|S_{11}|^2, G=|S_{12}|^2, B=|S_{22}|^2$

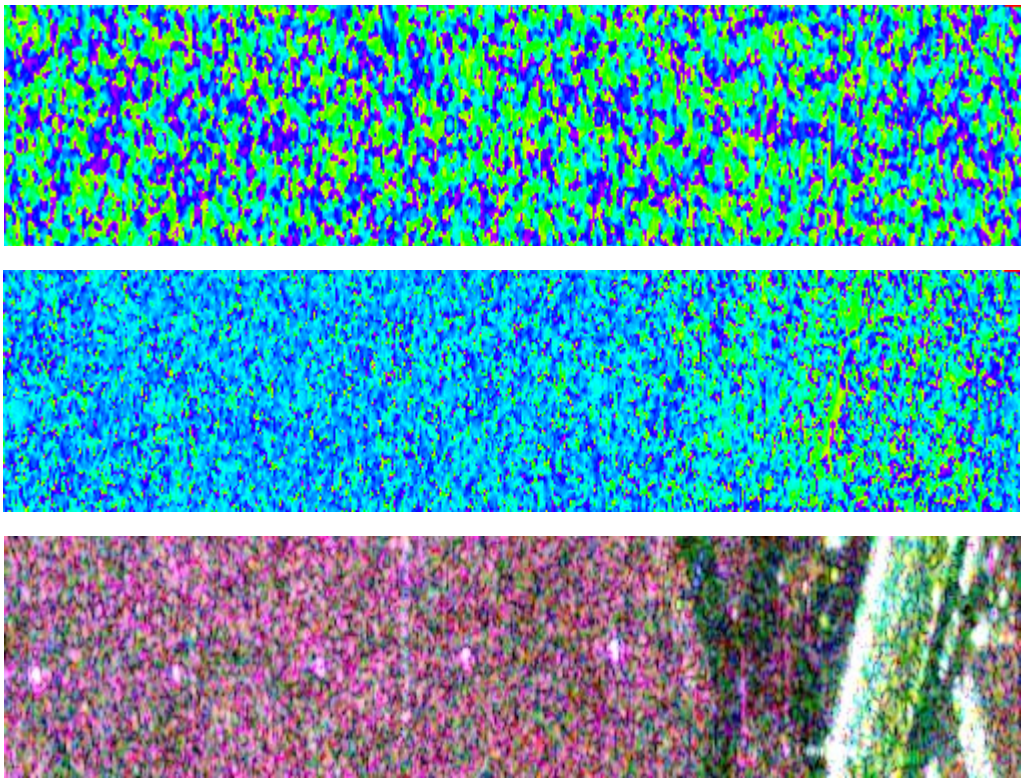

Fig. 4: $Arg(S_{11})$ (top) and $Arg(S_{11}S_{22}^{*})$ (middle) images.
Color coded image $R = |S_{11}|^2, G = |S_{12}|^2, B = |S_{22}|^2$ (bottom)

Speckle corrupts polarimetric observables (phase and intensity) in an important way. Specific procedures have to be used to retrieve relevant polarimetric information and to reduce the randomness of the acquired signals.

3.2 SIMPLE SPECKLE MODEL

3.2.1 SINGLE-POLARIZATION MULTIPLICATIVE SPECKLE MODEL

Speckle confers a random aspect to SAR images, but may not be considered as a simple noise. It is, in fact, tightly related to SAR measurement principle. [Goze 1993], [Lee 1980], [Lee 1981a], [Lee 1981b], [Lee 1983], [Lee 1986a], [Lee 1986b], [Lee 1994], [Lee 1997], [Lopes 1990], [Lopes 1993], [Touzi 1994].
Synthesized SAR data may be considered as the result of the integration of a scene coherent response within each resolution cell, resulting from the convolution of the SAR impulse response with the coherent contribution of each elementary scatterer, as illustrated in Fig. 5. As the number of contributing scatterers, within a resolution cell, tends to be large (it is the case for common resolution SAR measurements), the resulting integrated response is random in phase and amplitude and is shown to follow, over homogeneous areas, a Normal distribution.

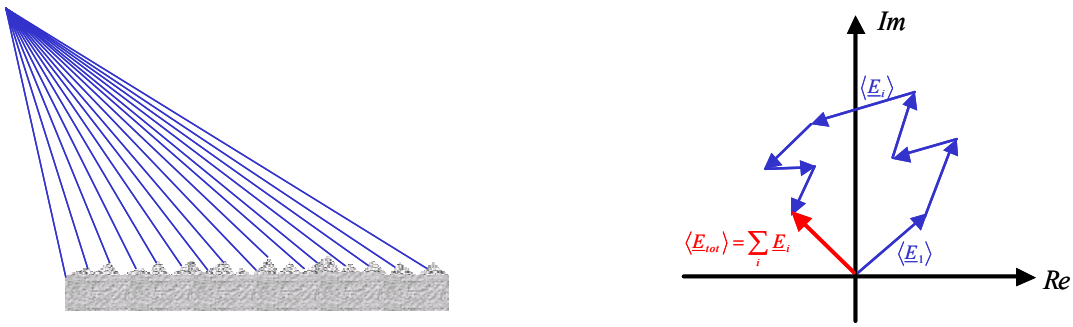

Fig. 5: Principle of coherent integration

A speckled response is usually represented under the form of a simple product model: $y = x.n$ where y represents a complex speckled scattering coefficient, x the original unspeckled scattering coefficient and n the multiplicative speckle contribution.
The speckle term, n is composed of independent real and imaginary parts, following both real centered Normal distribution $N_C(0, 1/2)$. The corresponding speckled intensity, Y, is

$$\begin{aligned} & Y = yy^* = xx^*\, nn^* \\ \Rightarrow \quad & Y = X\, nn^* \end{aligned} \tag{43}$$

Over homogeneous areas, X is considered to be constant and the speckled intensity follows an exponential probability density function

$$p(Y) = X^{-1} e^{-\frac{Y}{X}} \tag{44}$$

Its first two moments are given by:

$$E(Y) = X\, E(nn^*) = X \qquad \text{with:} \quad Var(Y) = X^2\, Var(nn^*) = X^2 \tag{45}$$

3.2.2 *POLARIMETRIC MULTIPLICATIVE SPECKLE MODEL*

This speckle model may be extended to the polarimetric case by considering that polarimetric channels are affected by independent multiplicative speckle components :

$$\begin{bmatrix} S_{11} \\ S_{12} \\ S_{22} \end{bmatrix} = \begin{bmatrix} x_{11} & & \\ & x_{12} & \\ & & x_{22} \end{bmatrix} \begin{bmatrix} n_{11} \\ n_{12} \\ n_{22} \end{bmatrix} \Rightarrow \begin{bmatrix} |S_{11}|^2 \\ |S_{12}|^2 \\ |S_{22}|^2 \end{bmatrix} = \begin{bmatrix} X_{11}(n_{11}n_{11}^*) \\ X_{12}(n_{12}n_{12}^*) \\ X_{22}(n_{22}n_{22}^*) \end{bmatrix} \tag{46}$$

One may note that the multiplicative assumption is in general not valid to model speckled correlation terms.

3.3 PRINCIPLE OF SCALAR SPECKLE FILTERING

3.3.1 *INCOHERENT AVERAGING*

As presented in the former paragraph, a speckled intensity, Y, may be considered as a random variable whose mean value equals the unspeckled intensity, X, but affected by a large variance.
The principle of speckle filtering consist in reducing the variance of Y in order to improve the estimate of its mean. The sample mean, $\langle Y \rangle$, is defined as the empirical average of L independent realizations of a speckled intensity as follows:

$$\langle Y \rangle = \frac{1}{L} \sum_{i=1}^{L} Y_i \tag{47}$$

It can be shown that, over homogeneous areas, this estimate of X follows a Gamma density function:

$$p(\langle Y \rangle) = \frac{L^L X \langle Y \rangle^{L-1}}{\Gamma(L) X^L} e^{-\frac{L\langle Y \rangle}{X}} \tag{48}$$

and has the following two first moments

$$E(\langle Y \rangle) = X \quad \text{with:} \quad Var(\langle Y \rangle) = X^2 / L \tag{49}$$

It is possible to observe from (49) that as the number of independent samples, L, reduces to 1 the variance of the estimate intensity increases, whereas incoherent averaging over L independent realizations permits to reduce the variance of a speckled intensity in a significant way. The quantity $L = \text{var}(I)/E(I)^2$ is called the Equivalent Number of Looks (ENL) and is a measure of speckle importance.

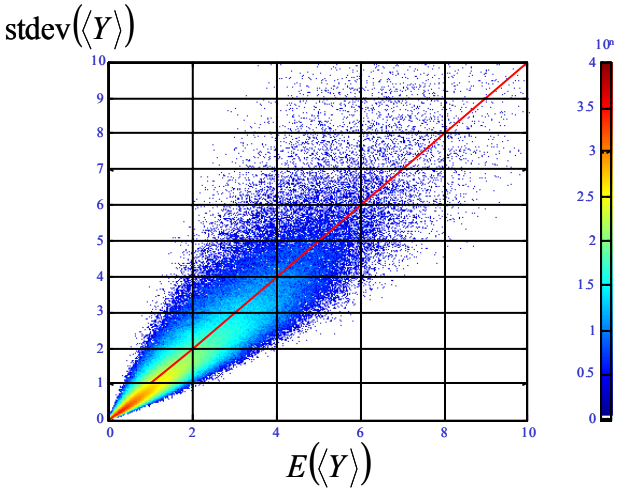

Fig. 6: Occurrence of single-look of intensity moments over a homogeneous areas

The occurrence plot displayed in Fig. 6 clearly shows that the standard deviation and the mean of sampled intensities are linearly related over homogeneous areas. The slope of this linear relation is $\sqrt{L}$ and equals 1 in the case of single-look data sets.

3.3.2 BOXCAR FILTER

The boxcar filter is a direct application of the incoherent averaging described by (47) to the case of an image. Filtered intensity estimates, $\widetilde{X}_{i,j}$, are constructed by computing the sample mean over each pixel neighborhood, defined by a sliding window of $(N_w \times N_w)$ pixels.

$$\widetilde{X}_{i,j} = \langle Y_{i,j} \rangle_{N_w} = \frac{1}{N_w^2} \sum_{p=-N_w/2}^{N_w/2} \sum_{q=-N_w/2}^{N_w/2} Y_{i+p,j+q} \tag{50}$$

where the subscripts i and j correspond to the considered pixel row and column index respectively. Fig. 7 shows an intensity image obtained using a (7×7) boxcar filter. This images shows enhanced contrast and lower random aspect.

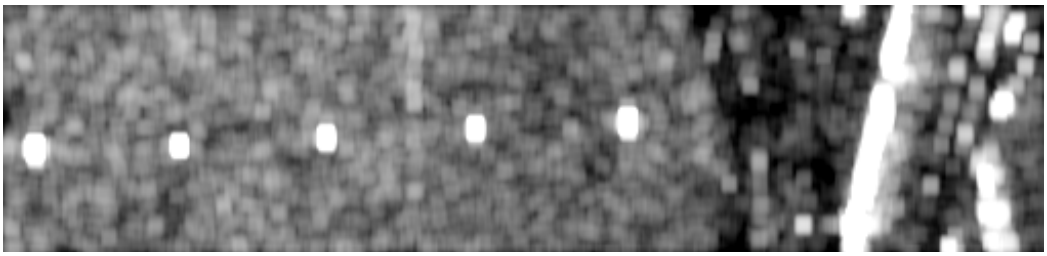

Fig. 7: $|S_{11}|^2$ filtered image using a boxcar filter

As it can be seen in Fig. 7, the boxcar filter is characterized by two main limitations :

- sharp edges are generally blurred
- point scatterers are over filtered and transformed to spread targets

Solutions to these limitations are offered by the refined Lee filter.

3.3.3 J.S. LEE ADAPTIVE FILTER

J. S. Lee's filter determines the unspeckled intensity estimate that minimizes a mean squared error [Lee 1980], [Lee 1981a], [Lee 1981b], [Lee 1983], [Lee 1986a], [Lee 1986b], [Lee 1994]:

$$\left\langle \left| \widetilde{X} - X \right|^2 \right\rangle \tag{51}$$

This MMSE filter is based on a linearized speckle model leading to the following estimate expression :

$$\widetilde{X} = \langle Y \rangle_{N_w} + k\left(Y - \langle Y \rangle_{N_w}\right) \tag{52}$$

where k is an adaptive filtering coefficient, based on local statistics, given by :

$$k = \frac{\mathrm{var}(X)}{\mathrm{var}\langle Y \rangle} = \frac{\mathrm{var}\langle Y \rangle - E^2\left(\langle Y \rangle\right)\sigma_n^2}{\mathrm{var}\langle Y \rangle[1+\sigma_n^2]} \tag{53}$$

with $\sigma_n^2 = \frac{1}{L}$ the a priori speckle variance. Over homogeneous areas, $\mathrm{var}(X) = 0 \Rightarrow k = 0$ and $\widetilde{X} = \langle Y \rangle_{N_w}$, whereas over point targets and highly heterogeneous areas, $k = 1 \Rightarrow \widetilde{X} = Y$ and the pixel intensity remains unaffected by the filtering procedure.

In order to reduce the sensitivity of the adaptive filtering coefficient, k, to isolated heterogeneities, this filter uses directional masks to determine the most homogeneous part of the sliding window where local statistics have to be estimated. This modification permits to preserve relatively sharp edges. [Lee 1994], [Lee 1997].

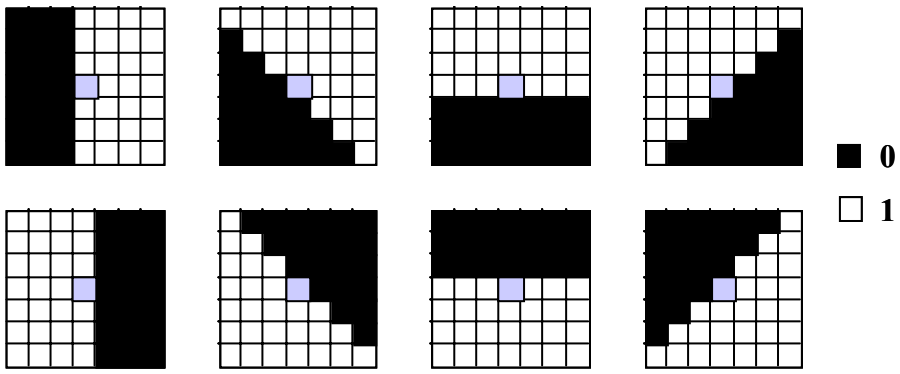

Fig. 8: Examples of directional masks

The Lee filter results displayed in Fig. 9 demonstrate the effectiveness of this adaptive filtering approach

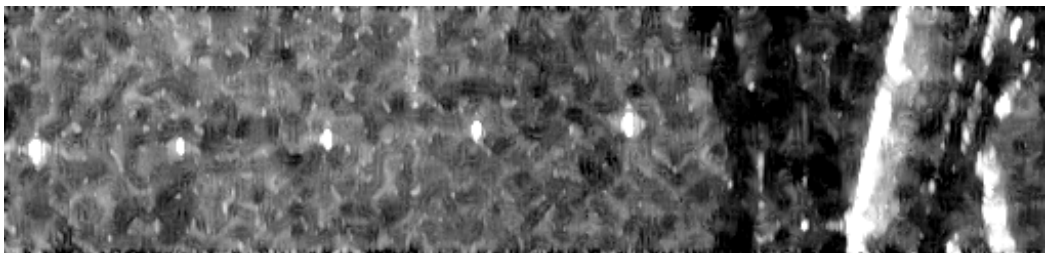

Fig. 9: $|S_{11}|^2$ filtered image using a (7×7) Lee filter

3.4 EXTENSION TO THE POLARIMETRIC CASE

Speckle filtering is based on incoherent averaging and requires to handle second order representations. The intensity information used in the scalar case has to be extended to the vector case when dealing with two or more polarization channels in order to take into account the different intensities as well as the cross-correlation related information. A simple way to build an incoherent polarimetric representation consists in vectorizing a scattering matrix to create a target vector and computing the corresponding (3×3) covariance matrix, $[C_3]$ or the (3×3) coherency matrix, $[T_3]$.

3.4.1 POLARIMETRIC BOXCAR FILTER

The extension of the boxcar filter to the polarimetric case is straightforward. The estimated covariance matrix is given by :

$$[\widetilde{C}]_{i,j} = \left\langle [C]_{i,j} \right\rangle_{N_w} = \frac{1}{N_w^2} \sum_{p=-N_w/2}^{N_w/2} \sum_{q=-N_w/2}^{N_w/2} [C]_{i+p,j+q} \tag{54}$$

where the subscripts i and j correspond to the considered pixel row and column index respectively.

3.4.2 J. S. LEE POLARIMETRIC FILTER

J. S. Lee proposed to estimate the unspeckled covariance matrix according to the following expression:

$$[\widetilde{C}] = \langle [C] \rangle + k\left([C] - \langle [C] \rangle\right) \tag{55}$$

where k remains a scalar coefficient computed from the span statistics, $span = C_{11} + C_{22} + C_{33}$.

This approximation is allows to filter polarimetric data in a fast and simple way and avoids additional coupling (or cross-talk) between the polarimetric channels. Fig. 10 shows improved color coded images processed through the boxcar and J. S. Lee filters.

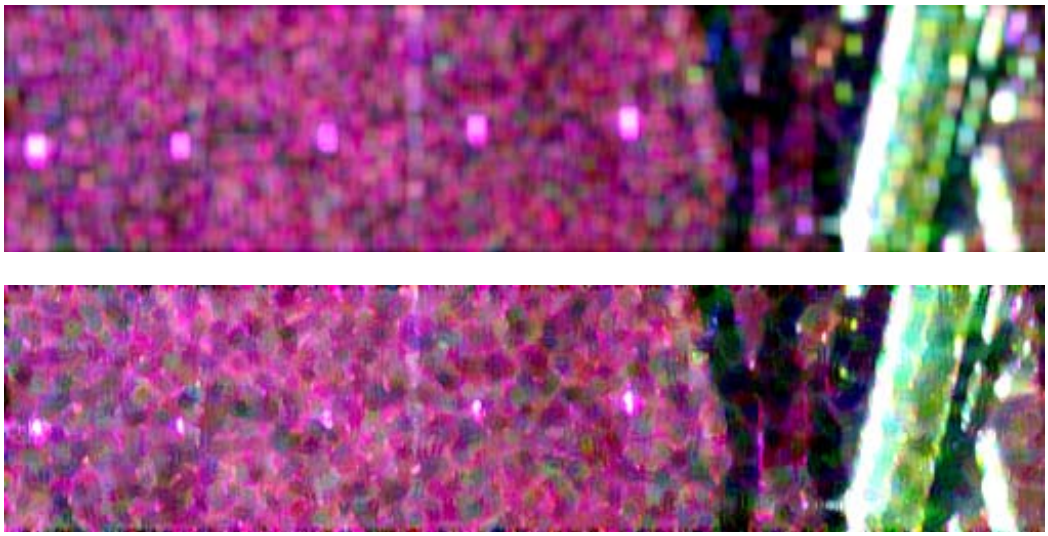

Fig. 10 : Color-coded, $R = |S_{11}|^2, G = |S_{12}|^2, B = |S_{22}|^2,$
filtered image using a (7×7) boxcar (top) Lee's filter (bottom)

3.5 CONSEQUENCES OF POLARIMETRIC SPECKLE FILTERING

It was seen in former paragraphs that it is necessary to reduce polarimetric variables random aspect by speckle filtering prior to any interpretation of polarimetric information. The incoherent averaging of the coherency [*T*] or covariance [*C*] matrices has an important impact on their polarimetric properties. Speckle filtering may cause a loss of polarimetric information by destroying the relation between and [*T*] or [*C*] matrices.

A coherency matrix is fully defined by 9 real coefficients: its three diagonal terms and three complex correlation coefficients. In the case of a single look coherency matrix, all three correlation coefficients have unitary modulus and one of their phase may be obtained by a linear combination of the remaining two, leaving 5 degrees of freedom. A relative scattering matrix $[S_{rel}]$ and single-look [*T*] or [*C*] matrices may be related in a unique way as shown in the following example :

$$[C] = \begin{bmatrix} C_{11} & C_{12} & C_{13} \\ C_{12}^* & C_{22} & C_{23} \\ C_{13}^* & C_{23}^* & C_{33} \end{bmatrix} = \begin{bmatrix} C_{11} & m_{12}e^{j\phi_{12}} & m_{13}e^{j\phi_{13}} \\ m_{12}e^{-j\phi_{12}} & C_{22} & m_{23}e^{j(\phi_{13}-\phi_{12})} \\ m_{13}e^{-j\phi_{13}} & m_{23}e^{-j(\phi_{13}-\phi_{12})} & C_{33} \end{bmatrix} \tag{56}$$

with $m_{ij} = \sqrt{C_{ii}C_{jj}}$, and :

$$[S_{rel}] = e^{-j\phi_1}[S] = \begin{bmatrix} \sqrt{C_{11}} & \sqrt{C_{22}/2}\,e^{-j\phi_{12}} \\ \sqrt{C_{22}/2}\,e^{-j\phi_{12}} & \sqrt{C_{33}}\,e^{-j\phi_{13}} \end{bmatrix} \tag{57}$$

The scattering mechanism may then be interpreted by comparing $[S_{rel}]$ to canonical examples. After speckle filtering, this may not be true anymore. In a general case, the modulus of correlation coefficients is inferior to one and the phase terms are linearly independent.

$$\left|\langle S_{ij}S_{kl}^*\rangle\right|^2 \le \langle |S_{ij}|^2\rangle\langle |S_{kl}|^2\rangle \qquad \text{and} \qquad Arg\left(\langle S_{ij}S_{kl}^*\rangle\right) \ne \langle Arg\left(S_{ij}S_{kl}^*\right)\rangle \tag{58}$$

In such a case, the coherency matrix is said to be **distributed** and cannot be related to a coherent scattering matrix.

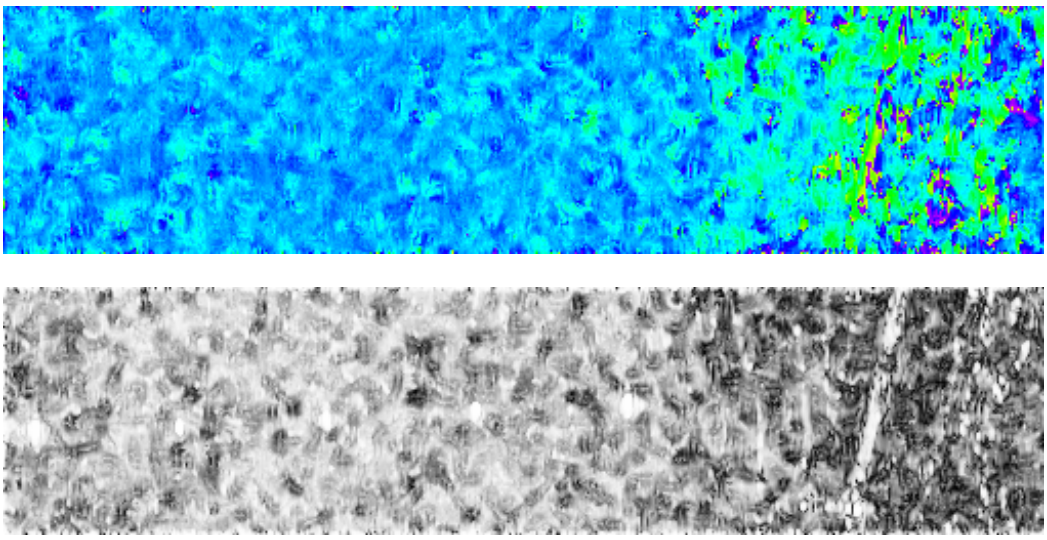

Fig. 11: Argument (top) and modulus (bottom) of $\left\langle S_{11}S_{22}^{*}\right\rangle / \sqrt{\left\langle \left|S_{11}\right|^{2}\right\rangle \left\langle \left|S_{22}\right|^{2}\right\rangle}$ *after application of a Lee filter*

The correlation coefficient displayed in Fig. 11 shows a varying modulus over the selected scene, indicating that the degree of correlation might be related to the nature of the scattering medium. The additional information contained in the cross-correlation terms will be exploited by **incoherent decomposition theorems** to extract even more characteristics from polarimetric data sets.

4 POLARIMETRIC TARGET DECOMPOSITION THEOREMS

There is currently a great deal of interest in the use of polarimetry for radar remote sensing. In this context, an important objective is to extract physical information from the observed scattering of microwaves by surface and volume structures. The most important observable measured by such radar systems is the 3x3 coherency matrix [*T*]. This matrix accounts for local variations in the scattering matrix and is the lowest order operator suitable to extract polarimetric parameters for distributed scatterers in the presence of additive (system) and/or multiplicative (speckle) noise.

Many targets of interest in radar remote sensing require a multivariate statistical description due to the combination of coherent speckle noise and random vector scattering effects from surface and volume. For such targets, it is of interest to generate the concept of an average or dominant scattering mechanism for the purposes of classification or inversion of scattering data. This averaging process leads to the concept of the « *distributed target* » which has its own structure, in opposition to the stationary target or « *pure single target* » [Huynen 1970][Pottier 1992].

Target Decomposition theorems are aimed at providing such an interpretation based on sensible physical constraints such as the average target being invariant to changes in wave polarization basis.

Target Decomposition theorems were first formalized by J.R. Huynen but have their roots in the work of Chandrasekhar on light scattering by small anisotropic particles. Since this original work, there have been many other proposed decompositions. We classify four main types of theorem:

1. Those employing coherent decomposition of the scattering matrix (Krogager, Cameron).
2. Those based on the dichotomy of the Kennaugh matrix (Huynen, Barnes).
3. Those based on a “model-based” decomposition of the covariance or the coherency matrix (Freeman and Durden, Dong).
4. Those using an eigenvector / eigenvalues analysis of the covariance or coherency matrix (Cloude, VanZyl, Cloude and Pottier).

A complete description of all these different Polarimetric Target Decomposition can be found in [Cloude 1996], and we focus here on the H / A / $\underline{\alpha}$ decomposition theorem which will be used further in the polarimetric classifications.

4.1 THE H / A / $\underline{\alpha}$ POLARIMETRIC DECOMPOSITION THEOREM

In 1997, *S.R. Cloude* and *E. Pottier* proposed a method for extracting average parameters from experimental data using a smoothing algorithm based on second order statistics [Cloude 1997]. This method does not rely on the assumption of a particular underlying statistical distribution and so is free of the physical constraints imposed by such multivariate models. An eigenvector analysis of the 3x3 coherency matrix [T] is used since it provides a basis invariant description of the scatterer and also provides a decomposition into types of scattering process (the eigenvectors) and their relative magnitudes (the eigenvalues). This original method, based on an eigenvalue analysis of the coherency matrix, employs a 3-level Bernoulli statistical model to generate estimates of the average target scattering matrix parameters. This alternative statistical model sets out with the assumption that there is always a dominant 'average' scattering mechanism in each cell and then undertakes the task of finding the parameters of this average component [Cloude 1997].

4.1.1 EIGENVECTOR-BASED DECOMPOSITION.

The instantaneous (single pixel) target return from a spatially extended target can be characterized either by its complex scattering matrix [S] which relates to received spatial-voltage, or by its 3x3 coherency matrix [T] which relates to spatial-power. In the case of spatial-averaging, it is customary to consider the expected value of the coherency matrix <[T]> as representing the averaged distributed target, as :

$$\langle [T] \rangle = \frac{1}{N} \sum_{i=1}^{N} \underline{k}_i \cdot \underline{k}_i^{*T} = \frac{1}{N} \sum_{i=1}^{N} [T_i] \tag{59}$$

From this estimate, the eigenvectors and eigenvalues of the 3x3 hermitian coherency matrix <[T]> can be calculated to generate a diagonal form of the coherency matrix which can be physically interpreted as statistical independence between a set of target vectors [Cloude 1992][Cloude 1996]. The coherency matrix <[T]> can be written in the form of:

$$\langle [T] \rangle = [U_3][\Sigma][U_3]^{-1} \tag{60}$$

where $[\Sigma]$ is a 3x3 diagonal matrix with nonnegative real elements, and $[U_3] = [\underline{u}_1 \quad \underline{u}_2 \quad \underline{u}_3]$ is a 3x3 unitary matrix of the SU(3) group, where $\underline{u}_1$, $\underline{u}_2$, and $\underline{u}_3$ are the three unit orthogonal eigenvectors.
By finding the eigenvectors of the 3x3 hermitian coherency matrix <[T]>, such a set of 3 uncorrelated targets can be obtained and hence a simple statistical model can be constructed, consisting of the expansion of <[T]> into the sum of 3 independent targets, each of which, represented by a single scattering matrix. This decomposition can be written following:

$$\langle [T] \rangle = \sum_{i=1}^{i=3} \lambda_i [T_i] = \sum_{i=1}^{i=3} \lambda_i \underline{u}_i \cdot \underline{u}_i^{*T} \tag{61}$$

where the real numbers λ_i are the eigenvalues of <[T]> and represent statistical weights for the three normalized component targets [T_i] [Cloude 1992].

If only one eigenvalue is nonzero then the coherency matrix <[T]> corresponds to a pure target and can be related to a single scattering matrix. On the other hand, if all eigenvalues are equal, the coherency matrix <[T]> is composed of three orthogonal scattering mechanisms with equal amplitudes, the target is said random and there is no correlated polarized structure at all.

Between these two extrema, there exists the case of partial targets and where the coherency matrix <[*T*]> has non-zero and non-equal eigenvalues. The analysis of its polarimetric properties requires a study of the eigenvalues distribution as well as a characterization of each scattering mechanism of the expansion.

To introduce the degree of statistical disorder of each target, the entropy (*H*) is defined in the Von Neumann sense from the logarithmic sum of eigenvalues of <[*T*]> [Cloude 1996][Cloude 1997], as:

$$H = -\sum_{i=1}^{i=3} P_i \, log_3(P_i) \tag{62}$$

where P_i are the probabilities obtained from the eigenvalues λ_i of <[*T*]> with:

$$P_i = \frac{\lambda_i}{\sum_{j=1}^{j=3} \lambda_j} \tag{63}$$

If the entropy *H* is low then the system may be considered as weakly depolarizing and the dominant target scattering matrix component can be extracted as the eigenvector corresponding to the largest eigenvalue and ignore the other eigenvector components.

If the entropy *H* is high then the target is depolarizing and we can no longer consider it as having a single equivalent scattering matrix. The full eigenvalue spectrum must be considered.

Further, as the entropy *H* increases, the number of distinguishable classes identifiable from polarimetric observations is reduced. In the limit case, when *H=1*, the polarization information becomes zero and the target scattering is truly a random noise process.

While the entropy is a useful scalar descriptor of the randomness of the scattering problem, it is not a unique function of the eigenvalue ratios. Hence, another eigenvalue parameter defined as the anisotropy *A* can be introduced, with :

$$A = \frac{\lambda_2 - \lambda_3}{\lambda_2 + \lambda_3} \tag{64}$$

When *A=0* the second and third eigenvalues are equal. The anisotropy may reach such a value for a dominant scattering mechanism, where the second and third eigenvalues are close to zero, or for the case of a random scattering type where the three eigenvalues are equal.

The condition for <[*T*]> to have such an equivalent scattering matrix [*S*] is for both the target entropy *H* and the anisotropy *A* to be equal to zero, which corresponds to a single nonzero eigenvalue (λ_1) [Cloude 1992][Cloude 1996]. In this case the coherency matrix <[*T*]> has rank *r=1*, and can be expressed as the outer product of a single target vector $\underline{k}_1$ with:

$$\langle [T] \rangle = \underline{k}_1 \cdot \underline{k}_1^{*T} = \lambda_1 \underline{u}_1 \cdot \underline{u}_1^{*T} \tag{65}$$

where $\lambda_1 = 2(A_0 + B_0)$ is equal to the Frobenius norm (Span) of the corresponding scattering matrix, and where the corresponding unit target vector is expressed as follows :

$$\underline{u}_1 = \frac{e^{j\phi}}{\sqrt{2A_0\lambda_1}}\begin{bmatrix} 2A_0 \\ C+jD \\ H-jG \end{bmatrix} = \frac{e^{j\phi}}{\sqrt{\lambda_1}}\begin{bmatrix} \sqrt{2A_0} \\ \sqrt{B_0+B}\; e^{+j\,arctan(D/C)} \\ \sqrt{B_0-B}\; e^{-j\,arctan(G/H)} \end{bmatrix} \tag{66}$$

It is interesting to note that the modulus of the three components of the unit target vector are directly function of the three « Huynen target generators ».

Without using ground truth measurements, this polarimetric parameterisation of the unit target vector $\underline{u}$ involves the fit of a combination of three simple scattering mechanisms : surface scattering, dihedral scattering and volume scattering, which are characterized from the three components (target generators) of the unit target vector such as:

Surface scattering: $A_0 >> B_0+B\ ,\ B_0-B$
Dihedral scattering: $B_0+B >> A_0\ ,\ B_0-B$
Volume scattering: $B_0-B >> A_0\ ,\ B_0+B$

4.1.2 *PROBABILISTIC MODEL FOR RANDOM MEDIA SCATTERING.*

In previous publications [Cloude 1995] [Cloude 1996] [Cloude 1997], a parameterisation of the eigenvectors of the 3x3 coherency matrix [*T*] has been introduced for the case of scattering medium which does not have azimuthal symmetry [Nghiem 1992], and which takes the form shown in (67).

$$\underline{u} = \begin{bmatrix} \cos\alpha & \sin\alpha\cos\beta\, e^{j\delta} & \sin\alpha\sin\beta\, e^{j\gamma} \end{bmatrix}^T \tag{67}$$

It follows a revised parameterisation of the coherency matrix [Cloude 1997], as :

$$\langle [T] \rangle = [U_3]\begin{bmatrix} \lambda_1 & 0 & 0 \\ 0 & \lambda_2 & 0 \\ 0 & 0 & \lambda_3 \end{bmatrix}[U_3]^{*T} \tag{68}$$

$$[U_3] = e^{j\phi_1}\begin{bmatrix} \cos\alpha_1 & \cos\alpha_2 e^{j\phi_2} & \cos\alpha_3 e^{j\phi_3} \\ \sin\alpha_1\cos\beta_1 e^{j\delta_1} & \sin\alpha_2\cos\beta_2 e^{j(\delta_2+\phi_2)} & \sin\alpha_3\cos\beta_3 e^{j(\delta_3+\phi_3)} \\ \sin\alpha_1\sin\beta_1 e^{j\gamma_1} & \sin\alpha_2\sin\beta_2 e^{j(\gamma_2+\phi_2)} & \sin\alpha_3\sin\beta_3 e^{j(\gamma_3+\phi_3)} \end{bmatrix} \tag{69}$$

The parameterisation of a 3x3 unitary matrix [U_3] in terms of column vectors with different parameters α_1 β_1 etc... is made so as to enable a probabilistic interpretation of the scattering process. In general, the columns of the 3x3 unitary matrix are not only unitary but mutually orthogonal. This means that in practice α_1 α_2 and α_3 are not independent.

In this case a statistical model of the scatterer is considered as a 3 symbol Bernoulli process i.e. the target is modeled as the sum of three [*S*] matrices, represented by the columns of [U_3] in (69), occuring with probabilities P_i ,given from (15) by the normalized eigenvalues so that $P_1 + P_2 + P_3 = 1$ [Cloude 1997].
In this way for example, the parameter α follows a random sequence:

$$\alpha = \{\alpha_1\alpha_2\alpha_3\alpha_2\alpha_1\alpha_2\alpha_3\alpha_1\alpha_1 \ldots\} \tag{70}$$

and the best estimate of this parameter is given by the mean of this sequence, easily evaluated as [Cloude 1997] :

$$\underline{\alpha} = P_1\alpha_1 + P_2\alpha_2 + P_3\alpha_3 \tag{71}$$

In this way, the *mean* parameters of the dominant scattering mechanism are extracted from the 3x3 coherency matrix as a mean target vector $\underline{u}_0$, such that:

$$\underline{u}_0 = e^{j\phi}\begin{bmatrix} \cos\underline{\alpha} \\ \sin\underline{\alpha}\cos\underline{\beta}\, e^{j\underline{\delta}} \\ \sin\underline{\alpha}\sin\underline{\beta}\, e^{j\underline{\gamma}} \end{bmatrix} \tag{72}$$

where the parameters $\underline{\alpha}$ $\underline{\beta}$ $\underline{\delta}$ and $\underline{\gamma}$ are defined in (19), and where ϕ is physically equivalent to an absolute phase.

4.1.3 THE ROLL INVARIANCE PROPERTY.

One of the most important property in Radar Polarimetry concerns the roll invariance. The effect of rotation around the radar line of sight [Cloude 1996] can be generated as:

$$\langle[T(\theta)]\rangle = \left[U_3^R\right]\langle[T]\rangle\left[U_3^R\right]^{-1} \tag{73}$$

where $\left[U_3^R\right]$ is the unitary similarity rotation matrix, given by:

$$\left[U_3^R\right] = \begin{bmatrix} 1 & 0 & 0 \\ 0 & \cos 2\theta & \sin 2\theta \\ 0 & -\sin 2\theta & \cos 2\theta \end{bmatrix} \tag{74}$$

According to the eigenvector-based decomposition approach, the coherency matrix can be written in the form of:

$$\langle[T(\theta)]\rangle = \left[U_3^R\right][U_3][\Sigma]\left[U_3\right]^{*T}\left[U_3^R\right]^{-1} = \left[U_3'\right][\Sigma]\left[U_3'\right]^{*T} \tag{75}$$

$$\left[U_3'\right] = \left[U_3^R\right][U_3] = e^{j\phi_1}\begin{bmatrix} \cos\alpha_1 & \cos\alpha_2 e^{j\phi_2'} & \cos\alpha_3 e^{j\phi_3'} \\ \sin\alpha_1\cos\beta_1' e^{j\delta_1'} & \sin\alpha_2\cos\beta_2' e^{j\left(\delta_2'+\phi_2'\right)} & \sin\alpha_3\cos\beta_3' e^{j\left(\delta_3'+\phi_3'\right)} \\ \sin\alpha_1\sin\beta_1' e^{j\gamma_1'} & \sin\alpha_2\sin\beta_2' e^{j\left(\gamma_2'+\phi_2'\right)} & \sin\alpha_3\sin\beta_3' e^{j\left(\gamma_3'+\phi_3'\right)} \end{bmatrix} \tag{76}$$

where $[\Sigma]$ is the same 3x3 diagonal matrix with nonnegative real elements. $\left[U_3'\right] = \left[\underline{v}_1 \quad \underline{v}_2 \quad \underline{v}_3\right]$ is the new 3x3 unitary matrix of the SU(3) group, where $\underline{v}_1$, $\underline{v}_2$, and $\underline{v}_3$ are the new three unit orthogonal eigenvectors.

Following the parameterisation of the 3x3 unitary matrix $[U'_3]$, it can be seen that the three parameters α_1 α_2 and α_3 remain invariant, as the three eigenvalues (λ_1 λ_2 λ_3).

It follows that the mean parameter $\underline{\alpha}$, and the two important scalar functions of the eigenvalues, the entropy H and the anisotropy A, are three **roll-invariant parameters**.

Among the *mean* parameters ($\underline{\alpha}$, $\underline{\beta}$, $\underline{\delta}$ and $\underline{\gamma}$) of the dominant scattering mechanism which can be extracted from the 3x3 coherency matrix, it is now clear from the above analysis, that for random media problems, the main parameter for identifying the dominant scattering mechanism is $\underline{\alpha}$. The three others parameters ($\underline{\beta}$, $\underline{\delta}$ and $\underline{\gamma}$) can be used to define the target polarisation orientation angle [Pottier 1998][Pottier 1999][Schuler 1999].

In previous publication [Cloude 1997], it has been shown that the useful range of the parameter $\underline{\alpha}$ corresponds to a continuous change from surface scattering in the geometrical optics limit ($\underline{\alpha}=0°$) through surface scattering under physical optics to the Bragg surface model, encompassing dipole scattering or single scattering by a cloud of anisotropic particles ($\underline{\alpha}=45°$), moving into double bounce scattering mechanisms between two dielectric surfaces and finally reaching dihedral scatter from metallic surfaces ($\underline{\alpha}=90°$).
The $\underline{\alpha}$ parameter estimate is related directly to underlying average physical scattering mechanism, and hence may be used to associate observables with physical properties of the medium [Cloude 1997]. Fig. 12 shows these three roll-invariant parameters : H, A and $\underline{\alpha}$.

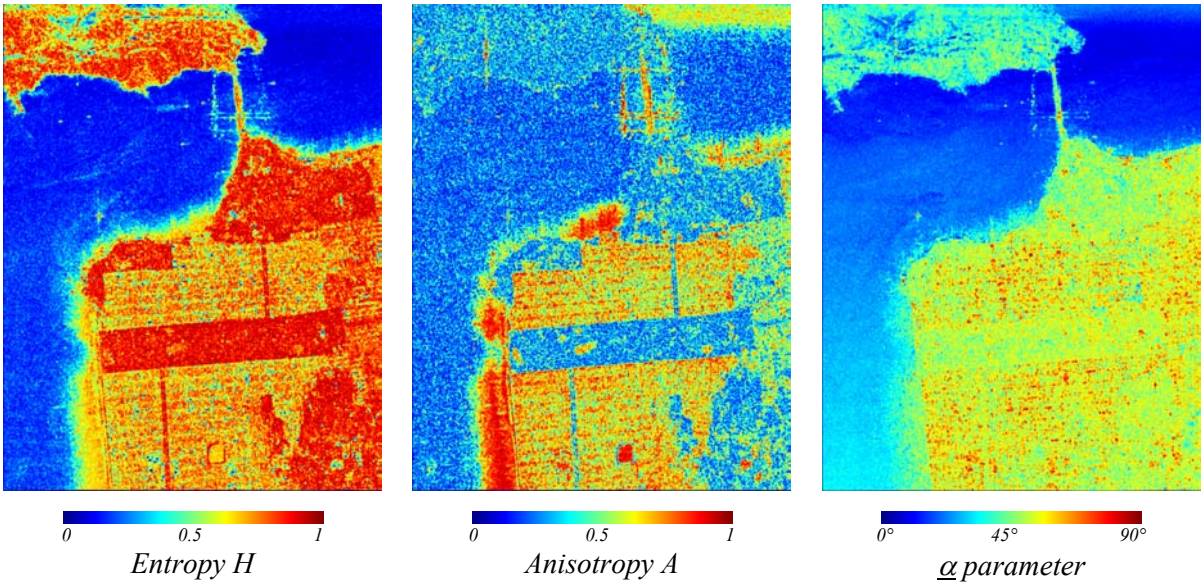

Fig. 12 : Roll-invariant parameters : H, A and $\underline{\alpha}$

The figure Fig. 12c corresponding to the $\underline{\alpha}$ parameter image shows that low value occurs over the ocean region, indicative of dominant single scattering ($\underline{\alpha} = 0°$). Urban area and parkland areas consist of medium and high $\underline{\alpha}$ parameter values ($45° < \underline{\alpha} < 90°$).

The figure Fig. 12a corresponding to the entropy image shows that low entropy scattering occurs over the ocean (scattering by a slightly rough surface). High entropy occurs over the parkland areas. At this resolution , the urban area consists of a mixture of low and high entropy processes, which are due to the different street/building classes which are aligned with the radar look direction, or aligned somewhat off boresight, or 45° aligned.

The figure Fig. 12b corresponding to the anisotropy image shows that low anisotropy scattering occurs both over the ocean region and parkland areas. The fact that the second and third eigenvalues are equal, corresponds either to a single dominant scattering mechanism or to a random scattering type. The urban area and the coastal sea consist of a mixture of medium and high anisotropy (presence of a second mechanism).

Although we can already identify several clear classes based on entropy alone, further information can be gleaned from the angle $\underline{\alpha}$ and from the anisotropy A, which can distinguish between the high entropy park and urban environments since the latter contains (moderate to high entropy) dihedral scattering.

4.1.4 THE THREE-DIMENSIONAL H / A / α CLASSIFICATION SPACE.

In previous publication [Cloude 1997], an unsupervised classification scheme has been introduced, based on the use of the two-dimensional $H / \underline{\alpha}$ classification plane, where all random scattering mechanisms can be represented. The key idea is that entropy arises as a natural measure of the inherent reversibility of the scattering data and that the alpha angle ($\underline{\alpha}$) can be used to identify the underlying average scattering mechanisms.
The $H / \underline{\alpha}$ classification plane is sub-divided into nine basic zones characteristic of classes of different scattering behavior, in order to separate the data into basic scattering mechanisms, as shown on Fig. 13a. The location of the boundaries within the feasible combinations of H and $\underline{\alpha}$ values is arbitrary and generically, i.e. based on the general properties of the scattering mechanisms. There is of course some degree of arbitrariness on the setting of these boundaries which are not dependent on a particular data set. This segmentation of the $H / \underline{\alpha}$ classification plane is offered merely to illustrate the unsupervised classification strategy and to emphasize the geometrical segmentation of physical scattering processes.
Complete details of the physical scattering characteristics of each of the nine zones can be found in [Cloude 1997][Pottier 2000].
The distribution of the San Francisco bay POLSAR data on the $H / \underline{\alpha}$ classification plane is shown on Fig. 13b.

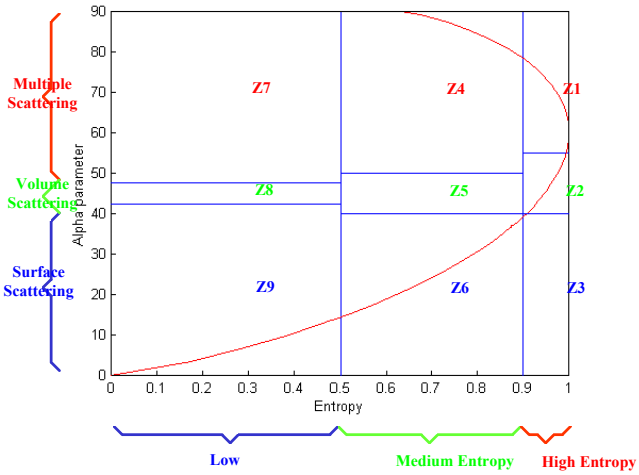

Fig. 13a : The H / α classification plane.

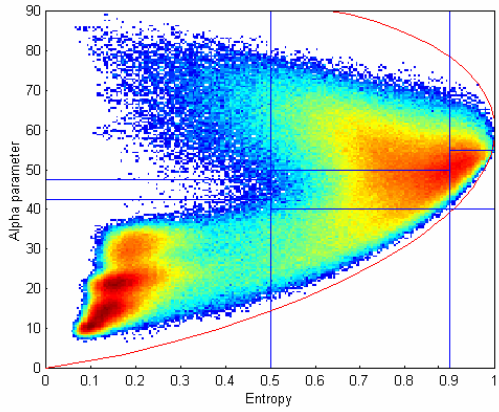

Fig. 13b : Polsar data distribution in the H / α classification plane.

Inherent of the spatial averaging, the entropy H may increase, and the number of distinguishable classes identifiable from polarimetric observations is reduced. For example, the feasible region of the $H / \underline{\alpha}$ classification plane is rapidly shrinking for high values of entropy ($H=0.9$), where $\underline{\alpha}$ parameter reaches the limited value of $60°$.

A high entropy, $H=0.9$, may correspond to two limit types of scattering process with associated eigenvalues spectra given, for example, by : $\lambda_1=1,\ \lambda_2=0.4,\ \lambda_3=0.4$ or by : $\lambda_1=1,\ \lambda_2=1,\ \lambda_3=0.3$.
To distinguish between these two different types of scattering process, it is necessary to introduce the anisotropy information, which takes the corresponding values $A=0$ and $A=0.54$ for the two previous examples.

In order to èxtend the classification scheme and to improve the capability to distinguish different types of scattering process, it is proposed to use some combinations between entropy and anisotropy information, as shown on Fig. 14. The .* operation represents the element by element multiplication of two matrices.

The examination of the different figures corresponding to the different combinations between entropy and anisotropy images leads to the following remarks :

1) - The *(1-H)(1-A)* image corresponds to the presence of a single dominant scattering process (low entropy and low anisotropy with $\lambda_2 \approx \lambda_3 \approx 0$).

2) - The *H(1-A)* image characterizes a random scattering process (high entropy and low anisotropy with $\lambda_2 \approx \lambda_3 \approx \lambda_1$)

3) - The *HA* image relates to the presence of two scattering mechanisms with the same probability (high entropy and high anisotropy with $\lambda_3 \approx 0$).

4) - The (1-*H)A* image corresponds to the presence of two scattering mechanisms with a dominant process (low to medium entropy) and a second one with medium probability (high anisotropy with $\lambda_3 \approx 0$).

These remarks are confirmed by the analysis of the distribution of the San-Francisco bay POLSAR data in the extended and complemented three-dimensional $H / A / \underline{\alpha}$ classification space, as shown on Fig. 6 This representation shows that it is possible to discriminate new classes using the anisotropy value.

For example, it is now possible to notice that there exists in the « Low Entropy Surface Scattering » area (Z9) a second class associated with a high anisotropy value and which corresponds to the presence of a second physical mechanism which is not negligible.

Identical remarks can be made concerning the « Medium Entropy Vegetation Scattering » area (Z5) and the « Medium Entropy Multiple Scattering » area (Z4). Due to the spread of the POLSAR data along the anisotropy axis, it is now possible to improve the capability to distinguish different types of scattering process which have quite the same high entropy value:

- High entropy and low anisotropy correspond to random scattering.
- High entropy and high anisotropy correspond to the presence of two scattering mechanisms with the same probability.

From the analysis of the different images shown on Fig. 14 and from the distribution of the San-Francisco bay POLSAR data in the $H / A / \underline{\alpha}$ classification space shown on Fig. 15., we can conclude that the anisotropy has to be considered now as a key parameter in the polarimetric analysis and/or inversion of POLSAR data.

The information contained in these three roll-invariant parameters extracted from the local estimate of the 3x3 hermitian coherency matrix $<[T]>$, corresponds to the type of scattering process which occurs within the pixel to be classified (combination of entropy H and anisotropy A) and to the corresponding physical scattering mechanism ($\underline{\alpha}$ parameter).

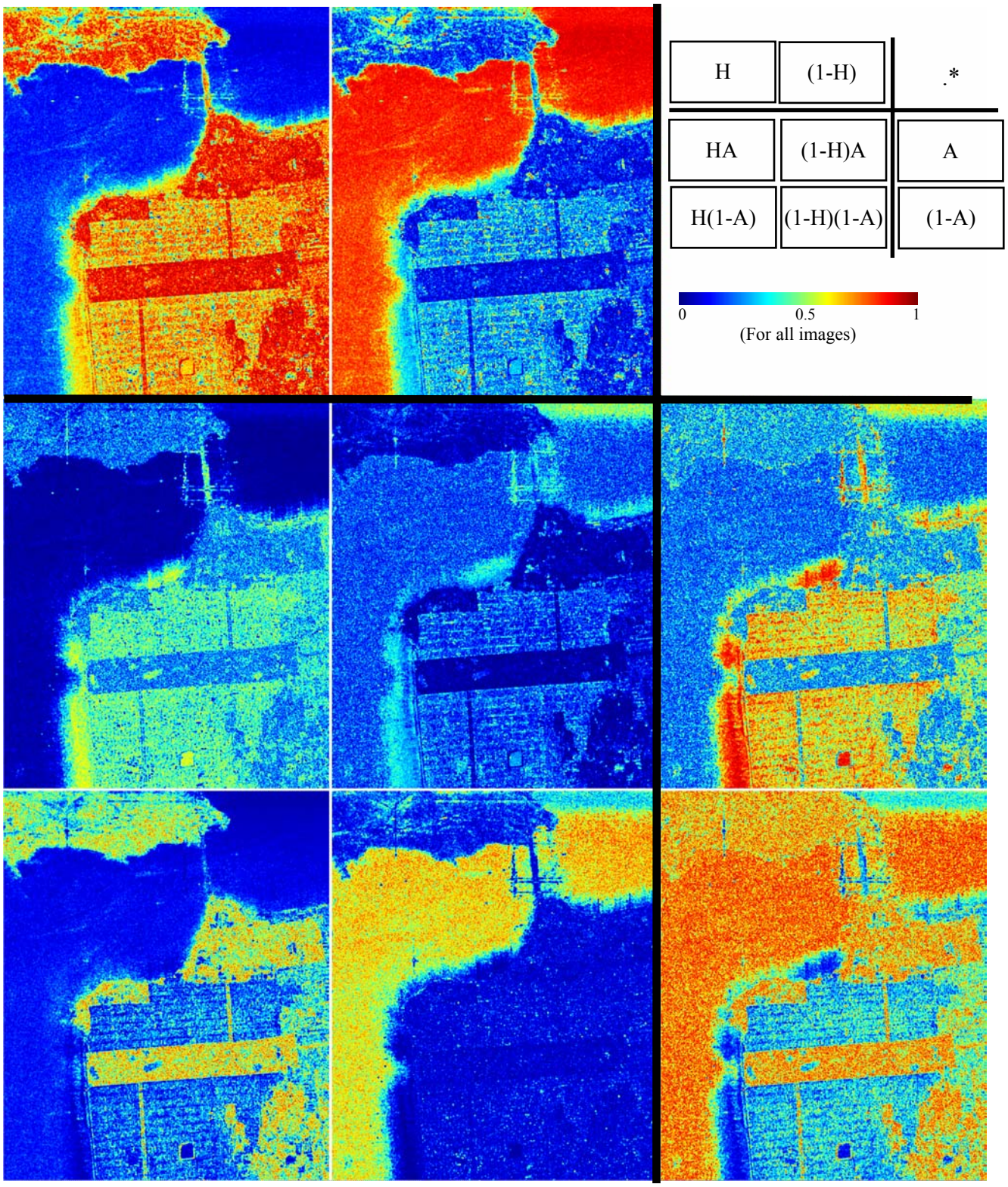

Fig. 14 : Combinations between entropy and anisotropy images.

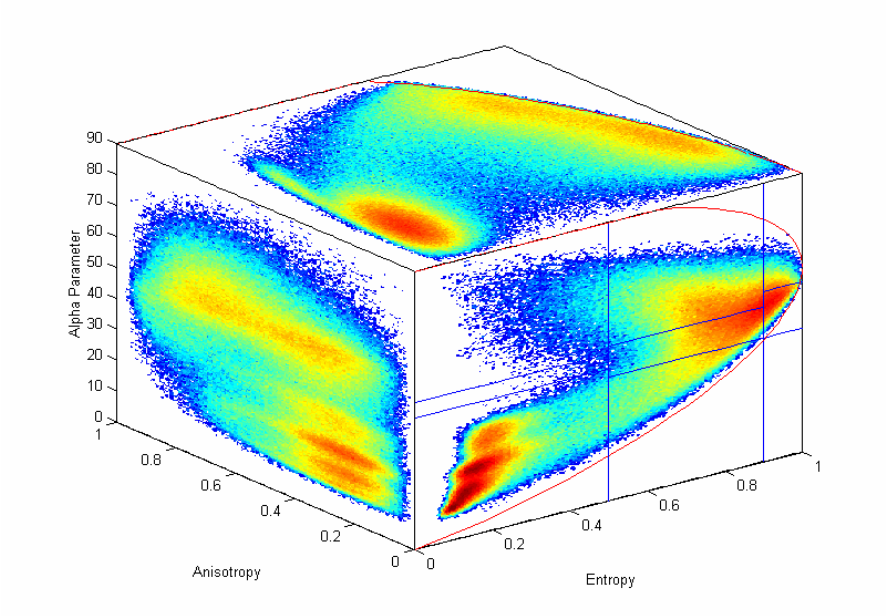

Fig. 15 : Distribution of the San-Francisco bay POLSAR data in the H / A / $\underline{\alpha}$ classification space

5 REFERENCES

(Common references to Part 1 and Part 2)

[Bamler 1998] R. Bamler, P. Hartl, "Synthetic Aperture Radar Interferometry", Inverse Problems, 14, R1-R54, 1998.

[Boerner 1998] W. M. Boerner et al "Polarimetry in Remote Sensing: Basic and Applied Concepts", Chapter 5 in Manual of Remote Sensing, Vol. 8, 3rd edition, F M Henderson, A J Lewis eds. New York, Wiley, 1998.

[Boerner 2000] W.M. Boerner, Y. Yamaguchi, "Extra Wideband Polarimetry, Interferometry and Polarimetric Interferometry in Synthetic Aperture Remote Sensing", Special Issue on Advances in Radar Systems, IEICE Trans. Commun., Vol. E83-B (9), Sept. 2000, pp 1906-1915.

[Chen 1996] K.S. Chen, W.P Huang, D. H. Tsay, F. Amar, "Classification of Multifrequency Polarimetric SAR Image Using a Dynamic Learning Neural Network," IEEE Transactions on Geoscience and Remote Sensing, vol. 34, no.3, 814-820, 1996.

[Cloude 1986] S.R. Cloude « Group theory and polarization algebra », *OPTIK*, vol. 75, n°1, pp 26-36, 1986.

[Cloude 1992] S.R. Cloude « Uniqueness of target decomposition theorems in radar polarimetry », *Direct and Inverse Methods in Radar Polarimetry, Part 1*, NATO-ARW, W.M. Boerner et al., Eds. New York : Kluwer Academic, 1992, pp 267-296.

[Cloude 1995] S.R. Cloude « Symmetry, Zero Correlations and Target Decomposition Theorems », Proceedings of *3rd International Workshop on Radar Polarimetry (JIPR '95)*, IRESTE, University of Nantes, March 1995, pp 58-68.

[Cloude 1996] S.R. Cloude, E. Pottier, "A Review of Target Decomposition Theorems in Radar Polarimetry", IEEE Transactions on Geoscience and Remote Sensing, Vol. 34 No. 2, pp 498-518, March 1996.

[Cloude 1997] S.R. Cloude, E. Pottier, "An Entropy Based Classification Scheme for Land Applications of Polarimetric SAR", IEEE Transactions on Geoscience and Remote Sensing, Vol. 35, No. 1, pp 68-78, January 1997.

[Cloude 1998] S.R. Cloude, K.P. Papathanassiou, "Polarimetric SAR Interferometry", IEEE Transactions on Geoscience and Remote Sensing, Vol 36. No. 5, pp 1551-1565, September 1998.

[Cloude 1999] S.R. Cloude, J. Fortuny, J.M. Lopez, A.J. Sieber, "Wide Band Polarimetric Radar Inversion Studies for Vegetation Layers", IEEE Transactions on Geoscience and Remote Sensing, Vol 37/2 No 5, pp 2430-2442, September 1999.

[Cloude 2000a] S.R. Cloude, K P Papathanassiou, W M Boerner, "The Remote Sensing of Oriented Volume Scattering Using Polarimetric Radar Interferometry", Proceedings of International Symposium on Antennas and Propagation, ISAP 2000, Fukuoka, Japan, pp 549-552, August 2000.

[Cloude 2000b] S.R. Cloude, K P Papathanssiou, W M Boerner "A Fast Method for Vegetation Correction in Topographic Mapping Using Polarimetric Radar Interferometry", Proceedings of 3rd European SAR Conference EUSAR 2000, Munich, Germany, pp 261-264, May 2000.

[Cloude 2001a] S.R. Cloude, I.H. Woodhouse, J. Hope, J.C. Suarez Minguez, P. Osborne, G. Wright,The Glen Affric Radar Project: Forest Mapping using dual baseline polarimetric radar interferometry, ESA Symposium on Retrieval of Bio and Geophysical Parameters from SAR for Land Applications, University of Sheffield, England, September 11-14, 2001.

[Cloude 2001b] S.R. Cloude, K P Papathanassiou, E. Pottier, "Radar Polarimetry and Polarimetric Interferometry", IEICE Transactions on Electronics, VOL.E84-C, No.12, 2001, pp1814-1822, December 2001.

[Cloude 2002] S.R. Cloude, K.P. Papathanassiou, "A 3-Stage Inversion Process for Polarimetric SAR Interferometry", Proceedings of European Conference on Synthetic Aperture Radar, EUSAR'02, pp. 279-282, Cologne, Germany, 4-6 June 2002.

[Desnos 1999] Y.-L. Desnos, H.Laur, P.Lim, P. Meisl, and T. Gach "The ENVISAT-1 Advanced Synthetic Aperture Radar Processor And Data Product," Proceedings of IGARSS'99, July 1999.

[Durden 1999] S.L. Durden, J.J. van Zyl, H.A. Zebker, "Modeling and Observations of the Radar Polarization Signatures of Forested Areas," IEEE Trans. Geoscience and Remote Sensing, vol. 27, no. 5, 2363-2373, September 1999.

[Ferro-Famil 2001a] L. Ferro-Famil, E. Pottier, J. S. Lee, "Unsupervised classification of multifrequency and fully polarimetric SAR images based on the H/A/Alpha-Wishart classifier", IEEE Transactions on Geoscience and Remote Sensing, vol. 39, n°11, pp 2332-2342, November 2001.

[Ferro-Famil 2001b] L. Ferro Famil, E. Pottier, "Dual Frequency Polarimetric SAR Data Classification and Analysis" in "Progress In Electromagnetics Research" Volume 24. J.A. Kong. Chief Editor, Ed. New York Elsevier, Vol. 24, pp 251-276, 2001.

[Ferro-Famil 2001c] L. Ferro-Famil, E. Pottier, J.S. Lee, "Unsupervised Classification and Analysis of Natural Scenes from Polarimetric Interferometric SAR Data," Proceedings of IGARSS-01, 2001.

[Ferro-Famil 2002] L. Ferro-Famil, E. Pottier, J.S. Lee, "Classification and Interpretation of Polarimetric SAR data", IEEE International Geoscience and Remote Sensing Symposium, June 2002, Toronto, Canada.

[Freeman 1998] A. Freeman, S. Durden " A three component scattering model for polarimetric SAR data ", IEEE Transactions on Geoscience and Remote Sensing, vol. 36, n°3, pp 963-973, May 1998.

[Goze 1993] S. Goze, A. Lopes, « A MMSE Speckle Filter for Full Resolution SAR Polarimetric Data », J.E.W.A., vol 7, n°5, pp 717-737, May 1993.

[Hajnsek 2000] I. Hajnsek, E. Pottier, S.R. Cloude, "Slope Correction For Soil Moisture and Surface Roughness Retrieval", Proceedings of 3rd European SAR Conference EUSAR 2000, Munich, Germany, pp 273-276, May 2000.

[Hajnsek 2003] I. Hajnsek, E. Pottier, S.R. Cloude, "Inversion of Surface Parameters from Polarimetric SAR", IEEE Transactions on Geoscience and Remote Sensing, vol. 31, n°4, pp 727-744, April 2003.

[Huynen 1970] J.R. Huynen « *Phenomenological theory of radar targets »,* Ph. D. dissertation, Drukkerij Bronder-offset, N.V. Rotterdam, 1970.

[Kong 1990] J.A. Kong, S. H. Yueh, R.T. Shin, J.J. van Zyl " Classification of Earth Terrain using Polarimetric Synthetic Aperture Radar Images ", Chapter 6 in *PIER Volume 3*, ed. J.A. Kong Elsevier 1990.

[Lee 1980] J.S. Lee, « Digital Image Enhancement and Noise Filtering by Use of Local Statistics », IEEE Transactions on Pattern Analysis and Machine Intelligence, Vol PAMI-2, n°2, pp 165-168, March 1980.

[Lee 1981a] J.S. Lee, « Refined Filtering of Image Noise Using Local Statistics », Computer Graphics and Image Processing, 15, pp 380-389, 1981.

[Lee 1981b] J.S. Lee, « Speckle Analysis and Smoothing of Synthetic Aperture Radar Images », Computer Graphics and Image Processing, 17, pp 24-32, 1981.

[Lee 1983] J.S. Lee, « A Simple Speckle Smoothing Algorithm for Synthetic Aperture Radar Images », IEEE Transactions on Systems, Man and Cybernetics, Vol SMC 13, n°1, pp 85-89, January/february 1983.

[Lee 1986a] J.S. Lee, « Speckle Suppression and Analysis for Synthetic Aperture Radar Images », Optical Engineering 25(5), pp 636-643, May 1986.

[Lee 1986b] J.S. Lee, M.R. Grunes, « Speckle Reduction in Multipolarization, Multifrequency SAR Imagery », IEEE Transactions on Geoscience and Remote Sensing, vol 29, n°4, pp 535-544, July 1991.

[Lee 1994a] J.S. Lee, K.W. Hoppel, S.A. Mango, A.Miller, "Intensity and Phase Statistics of Multi-Look Polarimetric and Interferometric SAR Imagery", IEEE Trans GE-32, pp. 1017-1028, 1994.

[Lee 1994b] J.S. Lee, M.R. Grunes, R. Kwok « Classification of multi-look polarimetric SAR imagery based on the complex Wishart distribution» International Journal of Remote Sensing, vol. 15, No. 11, pp 2299-2311. 1994.

[Lee 1994c] J.S. Lee, I. Jurkevich, P. Dewaele, P. Wambacq, A. Oosterlinck. « Speckle Filtering of Synthetic Aperture Radar Images: A Review », Remote Sensing Review, 1994, Vol n°8, pp 313-340.

[Lee 1995] J.S. Lee, and M.R. Grunes, "Statistical Analysis and Segmentation of Multi-look SAR Imagery Using Partial Polarimetric Data," Proceedings of IGARSS'95, 1422-1424, 1995.

[Lee 1999a] J.S. Lee, M.R. Grunes, G. De Grandi "Polarimetric SAR Speckle Filtering and its Implications for Classification", IEEE Transactions on Geoscience and Remote Sensing, Vol. 37, no. 5, pp. 2363-2373, September 1999.

[Lee 1999b] J.S. Lee, M.R. Grunes, T.L. Ainsworth, L.J. Du, D.L. Schuler, S.R. Cloude, "Unsupervised Classification using Polarimetric Decomposition and the Complex Wishart Distribution", IEEE Transactions Geoscience and Remote Sensing, Vol 37/1, No. 5, p 2249-2259, September 1999.

[Lee 2000] J.S. Lee, D.L. Schuler, T.L. Ainsworth, "Polarimetric SAR Data Compensation for Terrain Azimuth Slope Variation", IEEE Transactions on Geoscience and Remote Sensing, Vol. 38, pp 2153-2163, September 2000.

[Lee 2004] J.S. Lee, M.R. Grunes, E. Pottier, L. Ferro-Famil, "Unsupervised Terrain Classification Preserving Polarimetric Scattering Characteristics", IEEE Transactions on Geoscience and Remote Sensing, Vol. 42, pp 722-732, April 2004.

[Lopes 1990] A. Lopes, R. Touzi, E. Nezry, « Adaptative Speckle Filters and Scene Heterogeneity », IEEE Transactions on Geoscience and Remote Sensing, vol 28, n°6, pp 992-1000, November 1990.

[Lopes 1993] A. Lopes, E. Nezry, R. Touzi, H. Laur, « Structure Detection and Statistical Adaptive Speckle Filtering in SAR Images », International Journal of Remote Sensing, 1993, Vol 14, n°9, pp 1735-1758.

[Meisl 2000] P. Meisl, A. Thompson, and A.P. Luscombe, "RADARSAT-2 Mission: Overview and Development Status," Proceedings of EUSAR'2000, 373-376, May 2000.

[Mette 2002] T. Mette, K.P. Papathanassiou, I. Hajnsek, and R. Zimmermann, ''Forest Biomass Estimation using Polarimetric SAR Interferometry'', Proceedings IGARSS'02 (CD-ROM), Toronto, Canada, 22-26 June 2002.

[Ngheim 1992] Ngheim, S.H. Yueh, R. Kwok, F.K. Li « Symmetry properties in Polarimetric Remote Sensing », *Radio Science*, Vol. 27. No. 5, pp 693-711 Oct 1992.

[Novak 1990] L. Novak, M.C. Burl, "Optimal Speckle Reduction in Polarimetric SAR Imagery", IEEE Transactions AES Vol. 26, pp. 293-305, March 1990.

[Papathanassiou 1999] K.P. Papathanassiou, *"Polarimetric SAR Interferometry",* Dissertation, 1999 February 25, TU Graz; ISRN DLR-FB-99-07, ISSN 1434-8454, DLR-HR, Oberpfaffenhofen, Obb., Germany, May 1999.

[Papathanassiou 2000] K.P. Papathanassiou , S.R. Cloude, A. Reigber, "Single and Multi-Baseline Polarimetric SAR Interferometry over Forested Terrain", Proceedings of 3rd European SAR Conference EUSAR 2000, Munich, Germany, pp 123-126, May 2000.

[Papathanassiou 2001] K.P. Papathanassiou, S.R. Cloude, 2001, "Single-baseline polarimetric SAR interferometry", IEEE Transactions on Geoscience and Remote Sensing,. Vol. 39, No 6, pp 2352-2363, November 2001.

[Papathanassiou 2002] K.P. Papathanassiou, I. Hajnsek, A. Moreira, S.R. Cloude, "Forest Parameter Estimation using a Passive Polarimetric Microsatellite Concept", Proceedings of European Conference on Synthetic Aperture Radar, EUSAR'02, pp. 357-360, Cologne, Germany, 4-6 June 2002.

[Pottier 1992] E. Pottier « On Dr J.R. Huynen's main contributions in the development of polarimetric radar techniques, and how the « radar targets phenomenological concept » becomes a theory », SPIE Vol 1748, Radar Polarimetry, pp 72-85, 1992.

[Pottier 1998] E. Pottier, "Unsupervised Classification Scheme and Topography Derivation from POLSAR data based on the H/A/α polarimetric decomposition" Proceedings of 4th International Workshop on Radar Polarimetry (JIPR '98), IRESTE, University of Nantes, France, pp 535-548, July 1998.

[Pottier 1999] E. Pottier, D.L. Schuler, J.S. Lee, T. Ainsworth, "Estimation of Terrain Surface Azimuthal / Range Slopes using Polarimetric Decomposition of POLSAR Data", IEEE International Geoscience and Remote Sensing Symposium. Hamburg, 28 June - 2 July 1999.

[Pottier 2000] E.Pottier, J.S. Lee "Unsupervised Classification Scheme of POLSAR Images Based on the Complex Wishart Distribution and the H/A/a Polarimetric Decomposition Theorem" 3th European Conference on Synthetic Aperture Radar, EUSAR 2000, Munich, 23-25 May 2000.

[Reigber 2000] A. Reigber, A. Moreira, "First Demonstration of Airborne SAR Tomography Using Multi-Baseline L Band Data", IEEE Transactions on Geoscience and Remote Sensing, Vol. 38, No 5, pp 2142-2152, September 2000.

[Reigber 2001] A. Reigber, K.P. Papathanassiou, S.R. Cloude, A. Moreira, "SAR Tomography and Interferometry for the Remote Sensing of Forested Terrain", Frequenz, 55, pp 119-123, March/April 2001.

[Rignot 1992] E. Rignot, R. Chellappa and P. Dubois, "Unsupervised Segmentation of Polarimetric SAR Data Using the Covariance Matrix" IEEE Transactions on Geoscience and Remote Sensing, Vol. 30, no. 4, pp. 697-705, July 1992.

[Schuler 1996] D.L. Schuler, J S Lee, G. De Grandi "Measurement of Topography using Polarimetric SAR Images", IEEE Transactions on Geoscience and Remote Sensing, Vol. GE-34(5), pp 1266-1277, 1996.

[Schuler 1999] D.L. Schuler, J.S. Lee, T.L. Ainsworth, E. Pottier, « Terrain Slope Measurement Accuracy Using Polarimetric SAR Data », Proceedings of IGARSS'99, Hamburg, July 1999.

[Touzi 1994] R. Touzi, A. Lopes, « The Principle of Speckle Filtering in Polarimetric SAR Imagery », IEEE Transactions on Geoscience and Remote Sensing, Vol 32, n°5, pp 1110-1114, September 1994.

[Treuhaft 1999] R.N. Treuhaft, S.R. Cloude, "The Structure of Oriented Vegetation from Polarimetric Interferometry", IEEE Transactions Geoscience and Remote Sensing, Vol 37/2, No. 5, p 2620, September 1999.

[Treuhaft 2000] R.N. Treuhaft, P. Siqueria, "Vertical Structure of Vegetated Land Surfaces from Interferometric and Polarimetric Radar", Radio Science, Vol. 35(1), pp 141-177, January 2000.

[VanZyl 1989] J.J. Van Zyl "Unsupervised Classification of Scattering Behaviour Using Radar Polarimetry Data", IEEE Transactions on Geoscience and Remote Sensing, Vol. 27, no. 1, pp. 36-45, July 1989.

[VanZyl 1990] J.J. van Zyl and H.A. Zebker, "Imaging Radar Polarimetry," Chapter 5, PIERS 3 Progress in Electromagnetic Research, J.A. Kong, Editor, Elsevier, March 1990.

[Wakabayashi 1998] H. Wakabayashi, N. Ito, and H. Hamazaki, "PALSAR System on the ALOS," Proc. SPIE EurOpt series, Sensors, Systems and Next Generation Satellite II, pp. 181-189, 1998.

[Yamada 2001] H-Y. Yamada, Y. Yamaguchi, E. Rodríguez, Y-J. Kim, W-M. Boerner, "Polarimetric SAR Interferometry For Forest Canopy Analysis by Using the Super Resolution", IEEE International Geoscience and Remote Sensing Symposium. Sydney, June 2001, pp 1101 -1103.